

DELFT UNIVERSITY OF TECHNOLOGY
Faculty of Electrical Engineering, Mathematics and Computer Science

BACHELOR'S THESIS

**Design and implementation of a power supply for MEMS
vaporizing liquid microthrusters**

July 17, 2019

Proposer / Supervisor:
dr. ing. H.W. van Zeijl

Chair:
dr. S.D. Cotofana

Author:
K. Lam
M. Mrahorović

Supervisor:
ir. B. Mansouri

Jury:
ing. F. van der Zwan
ir. A. Montagne

Abstract

This thesis presents the design of an accurate current source for MEMS vaporizing liquid microthrusters. An analysis of different power supplies is presented. The design choices leading to the implemented current sink topology is given. The main components, which are an op-amp, a MOSFET and a resistor, are analyzed extensively. System integration tests showed that the current source worked adequately. The current source has also been tested separately and the imposed accuracy requirement is not met. The reason for this has to be further investigated, as there are many potential sources of errors which can cause deviations in the order of microampere. Lastly, several recommendations are given for improving the system.

Preface

This thesis was written for the Bachelor Graduation Project. With four other ambitious students, we spent valuable and educational time in the lab room. We have worked on the design of a data-acquisition and control system for a MEMS vaporizing liquid microthruster.

We would like to express our gratitude to dr. ing. Henk van Zeijl for setting up this project and to ir. Brahim el Mansouri and the designer of the thrusters Alisher Kurmanbay for assisting us through the project. Furthermore, we would like to thank dr. ir. Chris Verhoeven for his help and lending us equipment and dr. ir. Ger de Graaf for lending us the IR-camera. Also, we would like to thank dr. Angelo Cervone and ing. Xavier van Rijnsoever for their time to attend our green-light assessment. Moreover, we would like to thank dr. ing. Lager for coordinating the BAP projects.

Finally, a special mention to express our gratitude to ir. Anton Montagne, for his passionate teaching of the subject 'Electronics' which taught us a lot, his energy, enthusiasm and time for guiding us through the project and answering our questions and his quick response on emails at critical moments during the project.

*Koen Lam and Mirza Mrahorović
Delft, July 2019*

Contents

Symbols, acronyms and software	v
1 Introduction	1
1.1 Background information	1
1.2 State-of-the-art analysis.	2
1.3 Project objective	2
1.4 Task division of project	3
1.5 Problem scope for the supply subgroup.	3
1.5.1 Technical review	3
1.6 Thesis synopsis	5
2 Program of requirements	6
2.1 Program of requirements for entire system	6
2.1.1 Scoping	6
2.2 Heater specifications	7
2.3 Design requirements	7
3 Design description	9
3.1 Overview	9
3.2 Digital-to-analog converter	9
3.3 Choice between current, voltage or power source.	10
3.3.1 Voltage source	10
3.3.2 Current source	11
3.3.3 Power source.	11
3.4 Design of the feedback network.	11
3.4.1 Transadmittance amplifier.	12
3.4.2 Transadmittance amplifier with a NPN transistor	13
3.4.3 Transadmittance amplifier with a MOSFET	13
3.5 Bandwidth analysis	14
3.6 Feedback resistor analysis.	15
3.6.1 Desired gain	15
3.6.2 Show-stopper values for the accuracy of the resistor	15
3.7 MOSFET analysis	16
3.7.1 MOSFET requirements.	16
3.7.2 Modelling the MOSFET	17
3.8 Op-amp analysis	17
3.8.1 Noise analysis	17
3.8.2 Modelling the operational amplifier	19
3.8.3 Gain-bandwidth analysis	19
3.9 System measurement method	20
3.10 Component requirements	20
3.10.1 Circuit requirement	20
3.10.2 Op-amp requirements	20
3.10.3 MOSFET requirements.	21
3.10.4 MOSFET desired specifications	21
3.10.5 Feedback resistor requirements	21
4 Implementation	22
4.1 Implementation of the feedback resistor	22
4.2 Choice of MOSFET	22
4.3 Choice of op-amp.	23

4.4	Prototype	23
5	Evaluation	24
5.1	Overview	24
5.2	Testing and results	25
5.2.1	Noise.	25
5.2.2	Accuracy of the circuit	25
5.2.3	Maximum response time of 24 μs when sense current is supplied	26
5.2.4	Maximum settling time of 10 μs	27
5.3	System integration	29
5.4	Assessment	29
6	Conclusion	30
6.1	Future work	30
A	Microthruster	32
B	Component list	33
C	Derivation the maximum feedback resistor drift	34
D	MOSFET nodal analysis	35
E	DAC measurements	37
F	Equipment	38

Symbols, acronyms and software

Symbols

- V_{gs} : gate-source voltage
- I_{ds} : drain-source voltage
- S_v : noise voltage spectral density
- S_i : noise current spectral density
- GB_{min} : minimum gain bandwidth product
- B : bandwidth

Acronyms

- ADC: Analog-to-digital converter
- DAC: Digital-to-analog converter
- LPM: Low-pressure microthruster
- MEMS: Micro Electro-Mechanical Systems
- Show-stopper: Action, condition, event, or problem that is serious enough to halt an activity, program, or process until it is resolved¹
- VLM: Vaporizing liquid microthruster
- VCVS: Voltage-controlled voltage source
- VCCS: Voltage-controlled current source
- CCVS: Current-controlled voltage source
- CCCS: Current-controlled current source
- SMD: Surface-mount device
- PCB: Printed circuit board
- Heater element = Heater device = Load
- Heating current: Current used for heating the heater
- Sensing current: Current used for measuring the resistance of the heater
- LSB: Least Significant Bit

Software

- MATLAB: numerical analysis environment
- SLICAP (symbolic linear circuit analysis program): MATLAB-based simulation tool used by us to set up and solve design equations for our electronic circuit.
- LTSPICE: electronic circuit simulator used by us to generate netlists of our circuits for analysis with SLICAP.

¹<http://www.businessdictionary.com/definition/show-stopper.html>

Introduction

Pico- and nanosatellites have increased in popularity over the years [1]. In 2018, 244 nanosatellites were launched and it is predicted that in 2023 already 703 nanosatellites will be launched [2]. Nanosatellites can be used in a wide variety of fields, such as space debris removal, formation flying or swarm missions. They are lightweight and low-cost, but usually lack propulsion capability. There is still much research to be done into the micro-propulsion system for these satellites. The need for further development of these systems is also mentioned in the technology roadmap set by NASA [3]. MEMS can play an important role in the creation of micro-propulsion systems.

1.1. Background information

Micro-propulsion systems have many different variations based on their working principle, ranging from solar sails, cold gas propulsion systems, electric propulsion systems and chemical propulsion systems [4]. This project focuses on the resistojet thruster, which falls in the category of electric propulsion systems. There are in general two main types of microresistojets: the vaporizing liquid microthruster (VLM) and low-pressure microresistojet (LPM) [5]. In this project, we work with a VLM that is part of research project.

A VLM generally consists of a resistive heating element and a liquid channel, as shown in Figure 1.1. Thrust is delivered by heating a gas or liquid, accelerating it through a nozzle and expelling it into space. In our case, the propellant is water. When the water is heated up and starts to boil, bubbles appear inside the channel. These bubbles form a layer of thermal insulation and affect the heat transfer from the heater to the channel. This in turn affects the temperature of the resistive element and the pressure in the channel. Therefore, the amount of steam generated tends to oscillate. As the thrust is dependent on the mass flow rate [6], unwanted variations in the temperature and pressure can therefore lead to a fluctuating thrust. Furthermore, uncontrolled heating could even cause thermal runaway and destroy the device. Therefore, controlling the temperature of the heater element is of paramount importance.

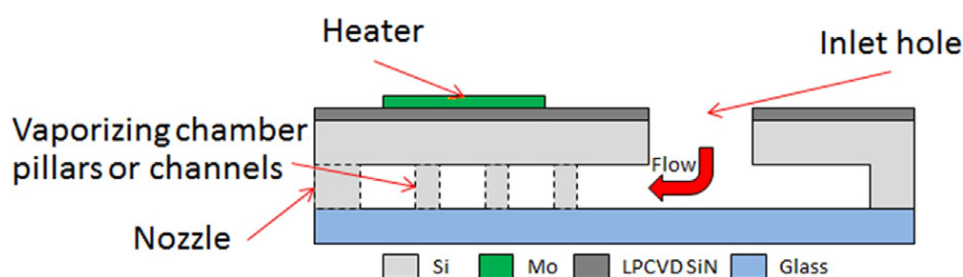


Figure 1.1: Schematic cross-section of the thruster taken from [6]

1.2. State-of-the-art analysis

Small satellites like CubeSats have several constraints that form a limitation in the design, e.g. its mass, dimensions, available power and propulsion [7]. Hence, there is a need for high performance, highly miniaturized and integrated micro-propulsion systems that meet these constraints [8].

Tummala and Dutta compared different micro-propulsion systems for CubeSats [9]. Their research shows that resistojets provide a relatively low specific impulse, have the highest average thrust-to-power ratio compared to other electric propulsion systems and can deliver a thrust between 0.1 mN and about 50 mN. This relatively low thrust can also be seen in the microresistojet propulsion concepts of Cervone, Zandbergen et al. [10]. In this work, the authors state that the presented concepts have the most potential in nanosatellite applications where a thrust between 0.5 mN and 10 mN is required. Due to their relatively low thrust, resistojets are also used on larger satellites for attitude control [9].

Controlling the thrust in magnitude and direction could make a big difference in the use of micro-propulsion systems [10]. A possible solution to control the thrust is to reduce bubble forming during heating. The transient behavior of bubble formation on micro-resistors is an active field of study [11]. Tsai and Lin have observed that the temperature of the heater rises with the increase of bubble size to reach a new equilibrium temperature, because it is believed that the heat dissipation path from the microresistor surface to the liquid is partially blocked by the vapor bubble. Several experiments have also been performed on microheaters to better understand the boiling process [12]. This project will attempt to control the temperature of the microheater and thereby also to control the bubbling process.

1.3. Project objective

In an attempt to stabilize the thrust, we have defined the following goals for the project:

1. To acquire data about the temperature of the heating element during dynamic liquid/vapor phenomenon.
2. To control the temperature of the heating element in an effort to reduce bubble forming.

To achieve these goals, we implement the required hardware and software compatible with multiple resistojets. These resistojets have pressure sensors integrated that create additional information about the system.

The microthruster is supposed to work in space on nanosatellites. However, this project is part of a research project on manufacturing microthrusters. Therefore, we assume that our system is only going to work on earth as a first prototype. Phenomena such as space radiation, high pressure and extreme temperature variations will be omitted and constraints such as limited space, limited power and extreme robustness will not be given priority in the design. This simplifies the design while providing valuable information to reach the objectives of the project.

The project can be considered a success if the following deliverables are accomplished.

1. Design and implementation of circuitry for real-time data acquisition from a heater array and from multiple EPCOS pressure sensors.
2. Design of front end data acquisition software.
3. Implementation of a control algorithm for temperature.

The results obtained from this project enable researchers to further investigate the effect of the bubble forming in microthrusters.

1.4. Task division of project

In order to reach the objectives of the project, the project is divided into subgroups. The temperature of the heater device is affected by supplying an electric input signal to the heater. The accuracy of this input signal determines the precision of the temperature which can be set. This is the challenge of the first subgroup: the supply group.

Implementing a feedback system poses some challenges, as there is no model available of the microthruster. Furthermore, effects such as the heat dissipation and stochastic bubble forming make modelling even more complex. Nonetheless, the need for an adequate feedback system is of uttermost importance for controlling the temperature. This is the focus of another subgroup: the control group.

Providing reliable input to the feedback system means that the resistance of the heater element should be read out accurately. The temperature dependency makes this a challenging task. Therefore, another subgroup is formed which tackles this challenge: the read-out subgroup.

A high level overview of the system is given in [Figure 1.2](#). To summarize, the following three subgroups are formed.

- Control: responsible for the control of the system.
- Read-out: responsible for the hardware read-out circuitry.
- Supply: responsible for the supply for the heater.

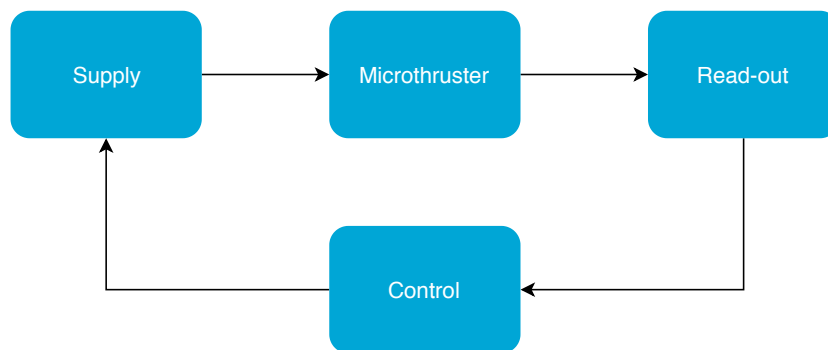


Figure 1.2: Overview of the subgroups

1.5. Problem scope for the supply subgroup

This thesis will present how an accurate supply for the microthruster can be implemented. It will be used for both heating up the resistive element of the microthruster as well as performing accurate measurements. The input of the supply is given by the control unit in the form of a voltage. The output of the supply is an electric signal with a certain amplitude, as determined by the control unit.

1.5.1. Technical review

There are several ways in which a supply for a resistive element can be made: a current source, a voltage source or a power source. A current source can be implemented in various ways. The simplest current source is a transistor. An operational amplifier is another example of an implementation of a current source, which among others consists of several transistors combined. Examples of current source implementations on the transistor level and with the use of op-amps can be found in [13] and [14]. Furthermore, many variations in the topology exist [15].

An interesting implementation of the current source is the current mirror, as shown in [Figure 1.3a](#), which keeps the output current through a load constant by copying the input current [15]. It consists of two transistors. This circuit has two disadvantages. First, the output current is not entirely independent of the output voltage, due to a non-infinite output impedance. Secondly, the transistors must be matched as accurately

as possible to reach ideal behaviour, which is a practical limitation. This current source has been used as a supply in a VLM [16].

To improve the current mirror composed of two transistors, the Wilson current source uses a third transistor, as shown in Figure 1.3b. The output impedance is increased, which overcomes the former limitation of the previous source. A third option would be to implement a cascode current mirror, which uses four transistors. However, self-heating can significantly affect BJT circuit behaviour in analog circuits [17]. To reduce this, the resistance in the base or emitter should be reduced or negative feedback should be applied. Furthermore, the limitation caused by accurate matching of the transistors remains. This leads us to consider other variants for a current source.

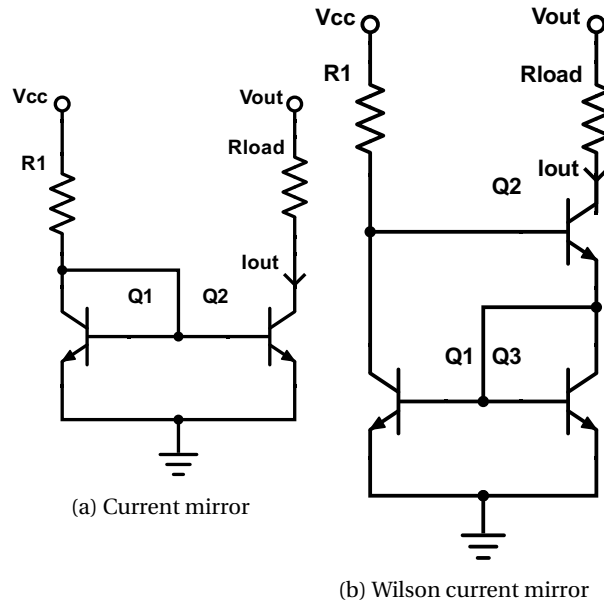


Figure 1.3: Current mirrors

Another interesting supply source is the Howland current pump, which is used as a voltage controlled current source. It consists of an op-amp combined with four resistors as shown in Figure 1.4. Howland current sources are used due to their simplicity, feasible implementation and superior driving capabilities [18]. However, due to resistor tolerances, the output resistance will not approach infinity and therefore the output current becomes dependent on the load voltage [19]. A modified Howland current pump, as shown in [20], also suffers from this limitation.

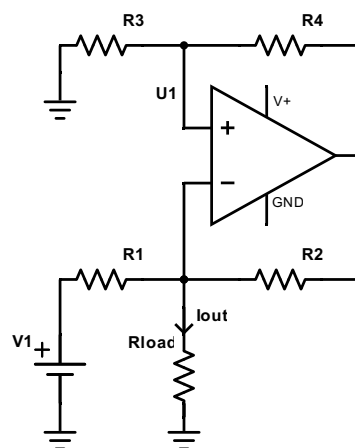


Figure 1.4: Howland current pump

A buck converter could also be used to supply the load. It steps down an input voltage to a lower output

voltage [21]. A basic buck converter consists of a switch, diode, inductor and resistor. A high efficient, non-inverting buck-boost DC-DC converter was presented by Gaboriault and Notman in [22]. The buck converter could be used to obtain a better power efficiency, which is further explained in [Section 6.1](#).

1.6. Thesis synopsis

The thesis starts with the requirements for the system in [Chapter 2](#). Then, the design decisions for the supply are elaborated in [Chapter 3](#). Next, the implementation of the system is explained. After that, the system will be tested and the results will be discussed in [Chapter 5](#). Lastly, we will assess our design and present recommendations for improvements in [Chapter 6](#).

2

Program of requirements

In this chapter, we first present the requirements for the entire system. Then, the heater specifications are given in [Section 2.2](#). Lastly, the requirements of the supply will be given and elucidated in [Section 2.3](#).

2.1. Program of requirements for entire system

The goal of the project is to design and implement a system which controls the temperature of the heater element in a resistojet and provides temperature and pressure readings. We have grouped the requirements of the system into several categories. Functional requirements describe what the system must have. The system requirements are limitations of the system and the safety requirements are set to prevent that the microthruster gets destroyed and ensure safety when testing. Lastly, the implementation requirement describes how the system should be built. The requirements can be found below. We have distinguished the mandatory requirements (MR) from the trade-off requirements (ToR).

2.1.1. Scoping

The microthruster is part of a research project and therefore, no clear requirements are known. We have thus decided to take overkill requirements. For the system, the overkill requirement is [Sys 1](#). It is not known beforehand which read-out precision we need to control the temperature within 10 °C and therefore, we set the bar high. Even if this read-out accuracy requirement of 1 °C is not met, experiments should be performed with our system to see whether a less strict read-out accuracy is also adequate to control the temperature within the given range.

Functional requirements

- | | | |
|-----------------------|--|-------|
| Sys 1 | The temperature read-out must have an accuracy of +/- 1 °C. | [MR] |
| Sys 2 | The temperature control must be within ± 10 °C of the set-point. | [MR] |
| Sys 3 | The resistor must be used as the heater. | [MR] |
| Sys 4 | The resistor must be used as the sensor. | [MR] |
| Sys 5 | The measurement needs to be a 4-probe measurement. | [MR] |
| Sys 6 | The system must have front-end data acquisition software. | [MR] |
| Sys 7 | The system needs to be able to make more than one measurement. | [MR] |
| Sys 8 | At least two EPCOS pressure sensors need to be read out. | [ToR] |
| Sys 9 | The system should preferably read out at least three thrusters. | [ToR] |

System requirements

- Sys 10** The circuit has to be portable. [MR]
- Sys 11** The system should not use more than 5 W. [ToR]
- Sys 12** The system should be able to be connected to different loads (i.e. thrusters) ranging from 100 to 1000 Ω . [ToR]

Safety requirements

- Sys 13** The maximum temperature that the resistor can withstand is around 300 $^{\circ}\text{C}$; the temperature should not become higher. [MR]
- Sys 14** The maximum voltage available is limited to 40 V. [MR]

Implementation requirement

- Sys 15** The system should preferably be implemented on a PCB. [ToR]

2.2. Heater specifications

The specifications of the microthruster depend on the device, as the resistance and temperature coefficient varies for each manufactured device. The resistance can vary between 100 Ω and 1000 Ω . In the design phase presented in [Chapter 3](#), we assumed worst-case scenarios in terms of a resistive load when deriving show-stopper values.

- S1** The load has a resistance between 100 Ω and 1000 Ω depending on the temperature of the heater.
- S2** The heater has a temperature coefficient of 0.0024 K^{-1} .
- S3** The maximum power available to the heater is 5 W.

2.3. Design requirements

The goal of this subsystem of the project is to design and implement an accurate electric supply. It is used to control the resistance and thereby the temperature of the heater device. The functional requirement for the complete system [Sys 2](#) is dependent on the accuracy of the supply. If the supply is not accurate due to noise (e.g. temperature drift, cables, connections), the resistance and thus the temperature cannot be regulated with precision. If this noise causes an error equivalent to 1 $^{\circ}\text{C}$ in the read-out, requirement [Sys 1](#) cannot be met. This requirement translates to an equivalent error in the current and voltage given by requirement [R5](#). The actual value is 525.6 μV , but for convenience, we have rounded this number to 500 μV . It is based on the maximum allowed noise voltage on the input of the ADC and takes the bandwidth of the system and resolution of the ADC into account. For a complete derivation, we would like to refer the reader to thesis [\[23\]](#).

Note that we have distinguished two types of electrical signals: a signal used for heating and a signal used for measuring. The signal used for measuring should not affect the temperature of the resistive element too much. Therefore, the signal used for measuring is lower in magnitude. Sensing and heating can be separated in the time domain or in the frequency domain [\[23\]](#). It leads to requirement [R1](#) for the supply unit in case the latter domain is preferred.

The supply must respond faster than the oscillations in temperature caused by the bubbling process. Therefore, the total delay in the system must be kept small. This delay consists of two parts; the output signal responds to the input signal after a certain delay and secondly, the output signal has a settling time. The settling time will be defined as the time that the desired output signal reaches up to 1 LSB of the final value. However, reading out 1 LSB will be very difficult. Thus, we will assume that when the output becomes steady (i.e. when the oscillations stop and the line is horizontal), the steady state is reached. The requirement for the total delay is given by [R6](#). Furthermore, because the input of the system comes from a microcontroller pin, it is required that the system can be controlled with a voltage signal (requirement [R2](#)).

Also important to note is that we have decided to focus on a heater device with a resistance of $660\ \Omega$. All specifications have been derived assuming a load resistance of $660\ \Omega$. The loads vary between $100\ \Omega$ to $1000\ \Omega$ and most of the devices available were in the range of $660\ \Omega$. Instead of choosing an extreme (e.g. $100\ \Omega$), we have decided to derive requirements for a $660\ \Omega$ load. During testing, we have used a resistance of $100\ \Omega$ to represent the load, because the voltage drop across the load would be within the range allowed in the lab room. During derivation of design requirements, we plugged the worst-case resistance values in the equations obtained, to ensure that the requirement would be met. Again, this is done on purpose, because the behaviour and parameters of our specific heater device are not known. Aiming for an extreme accuracy requirement in order to ensure that the temperature can be read-out and controlled accurately (i.e. within $10\ ^\circ\text{C}$) takes away the risk of underestimating the oscillations in temperature due to the bubbling process. This explains the overkill taken in the requirements.

Translating the heater specification S3 into a current and voltage, assuming that the load has a resistance of $660\ \Omega$, leads to a maximum heating current through the load of $87\ \text{mA}$. Or, a maximum heating voltage across the load of $57\ \text{V}$. However, for this specification we want to have some margin in the design. Therefore, the maximum heating current is $100\ \text{mA}$ and the maximum heating voltage is $70\ \text{V}$ (requirement R3). During sensing, the temperature of the heater device should stay unaffected. Because the duration of the pulse is short, we assumed that $50\ \text{mA}$ or $35\ \text{V}$ will not affect the temperature of the system in such a way that it will be detrimental for controlling. This gives rise to requirement R4. Lastly, we would like to minimize the influence of variations in load resistance on the output current or voltage (requirement R7).

The requirements are:

- R1 The supply has to be able to deliver a frequency signal.
- R2 The supply has to be controlled with a voltage signal.
- R3 The system has to be able to supply a heating current through the load of $100\ \text{mA}$. Or, a heating voltage across the load of $70\ \text{V}$.
- R4 The system has to be able to supply a sensing current through the load of $50\ \text{mA}$. Or, a sensing voltage across the heater of $35\ \text{V}$.
- R5 The noise in the system should not cause an error more than $500\ \mu\text{V}$ over the load.
- R6 During sensing (i.e. when a current of $50\ \text{mA}$ or voltage of $35\ \text{V}$ is supplied), the time between a change in the input of the system and the output settling to 1 LSB should be less than $34\ \mu\text{s}$.
- R7 Influence of variations in load resistance on the output current should be minimized.

3

Design description

In this chapter, the design choices for the power supply will be elaborated. First, a high level overview of the designed system and a brief explanation of how it operates are given in [Section 3.1](#). Next, we will compare three different types of sources in [Section 3.3](#): voltage, current and power source. Based on these findings, we will explain which type of source we chose. Then, we will present the design of the feedback network in [Section 3.4](#). After that, each component of the circuit will be analysed in [Section 3.6](#), [Section 3.7](#) and [Section 3.8](#). This analysis will explain how the show-stopper values for each of the components were derived. Finally, we will summarize the obtained show-stopper values for the components in [Section 3.10](#).

3.1. Overview

[Section 3.1](#) shows a schematic of the final design. Three different parts of the circuit can be observed: the digital to analog conversion, the supply circuit and the analog to digital conversion. The DAC is used to translate a digital signal to an analog signal and is explained in [Section 3.2](#). The ratio of the DAC voltage divided by R_F sets the current through R_{load} , which is the resistive element of the microthruster. Hence, the DAC output voltage sets the desired current through the load.

As can be seen from [Figure 3.1](#), there are two resistors of which the voltage across is measured. R_F is a precision resistance which, unlike R_{load} , has a low temperature coefficient (i.e. the variations in resistance due to temperature are small). Dividing the voltage measurement at R_F by the resistance of R_F gives the current flowing through R_F and consequently also the current through the load. Dividing the voltage measurement at R_{load} by either the measured current, or the current ratio $\frac{V_{DAC}}{R_F}$, gives the resistance of the load. This resistance value is fed back to the control unit, which ultimately decides whether the current through the load should be increased or decreased. This, in turn, affects the temperature and therefore the resistance. An explanation of this analog-to-digital conversion can be found in [\[23\]](#).

Before explaining the design of the supply circuit, the digital-to-analog conversion step will be elucidated.

3.2. Digital-to-analog converter

The digital-to-analog converter is used to translate a signal from the digital domain, coming from the control unit, to the analog domain, which serves as the input signal for the supply unit. The communication with the controller is done via SPI. The DAC is connected to a voltage reference of 1.024 V. This gives more stability and accuracy. How the ADC is controlled can be read in [\[24\]](#). [Appendix E](#) contains figures which justify that the DAC works.

There are many high accuracy and low-cost off-the-shelf ADCs available. Hence, the design will not focus on this part. We will assume that a reliable and instantaneous voltage signal can be supplied from the ADC. Furthermore, from the datasheet, which can be found in [Appendix B](#), it followed that the output impedance is 0.015Ω . We assumed that this is the only noise source in the DAC. By designing the supply unit with enough

tolerance in terms of noise and speed (response time and settling time), we assumed that the ADCs noise and response time will not be detrimental to the system.

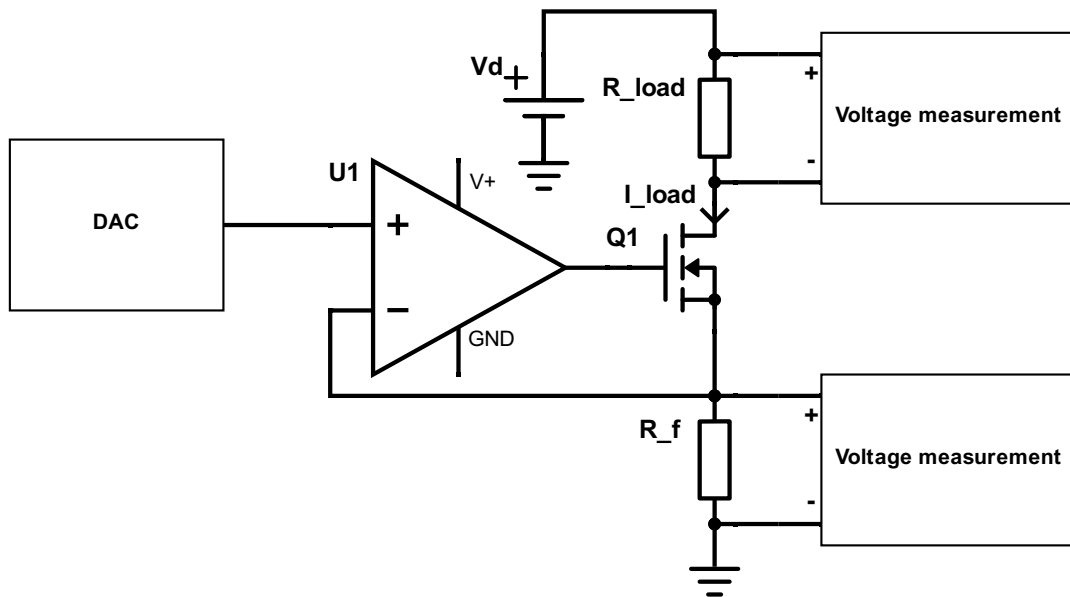


Figure 3.1: Overview of the system

3.3. Choice between current, voltage or power source

According to specification S1, the heater element (also called load) has a resistance between $100\ \Omega$ and $1000\ \Omega$ depending on the temperature of the heater. The source also has to be voltage controlled according to requirement R2.

3.3.1. Voltage source

An ideal voltage source can maintain a fixed voltage across a load irrespective of the load resistance. When a voltage source is used as supply, the current through the load must be measured to determine the resistance. A practical voltage source has the following advantages and disadvantages with respect to other types of sources:

Advantages

- + A voltage source is easier to implement than a current or power source.
- + There is no thermal runaway¹, since the heater has a positive temperature coefficient according to specification S2.

Disadvantages

- The resistance can be calculated using Ohm's law: $R = \frac{V}{I}$. Note that the measured current I is in the denominator. Therefore, if the current measurement has Gaussian noise, the resistance will have non-Gaussian noise.
- Measuring current through the load is more difficult than measuring the voltage to determine the resistance.

¹i.e. when an increase in temperature of an element leads to a further increase in temperature

3.3.2. Current source

An ideal current source delivers a fixed current to a load irrespective of the load resistance. It has the following advantages and disadvantages:

Advantages

- + With some measurement voltage noise, the noise of the resistance will also be Gaussian.
- + Voltage is easier to measure than current.
- + When testing the current source at 100 mA, a smaller load resistor can be used. This means that the full range of the current source can be tested while staying within the 40 V safety limit.

Disadvantages

- A current source is harder to implement than a voltage source.
- There will be thermal runaway due to the positive temperature coefficient of the heater.

3.3.3. Power source

A power source has to following advantages and disadvantages:

Advantages

- + The heater will always receive the maximum power.

Disadvantages

- A power source is more difficult to implement than a voltage or current source.
- Both current and voltage have to be measured to determine the resistance.

Since accurate resistance measurements are needed and because of the fact that a voltage across a load is easier to measure, a current source is chosen to supply the heater.

3.4. Design of the feedback network

We have thus chosen for a voltage-controlled current source. The design for a voltage-controlled current source or transadmittance amplifier starts with the feedback topology with a nullor [25]. A nullator is defined as an element having zero voltage across its terminals. A norator is an element which can have an arbitrary current and voltage between its terminals. Starting with the basics, we have a voltage at the input and wish to have a current at the output. Therefore, to implement feedback, we must convert the output current to a voltage and compare it to the supplied input voltage. Figure 3.2a shows that the resistance R_f is used for that. The norator in Figure 3.2a functions to supply the desired current through the load. The nullator and norator combined form a nullor.

The nullor is an ideal component. In order to make the circuit practical, we must switch to an operational amplifier. In this feedback topology, the nullor cannot be directly replaced with an op-amp, since for an op-amp the norator has to have a connection to ground. In order to resolve this constraint, the load resistor R_{load} must be placed under the norator and above resistor R_1 as in Figure 3.2b. The desired transfer matrix of the input voltage and current to the output voltage and current is given by Equation 3.1.

$$\begin{bmatrix} V_{in} \\ I_{in} \end{bmatrix} = \begin{bmatrix} 0 & R_F \\ 0 & 0 \end{bmatrix} \begin{bmatrix} V_{out} \\ I_{out} \end{bmatrix} \quad (3.1)$$

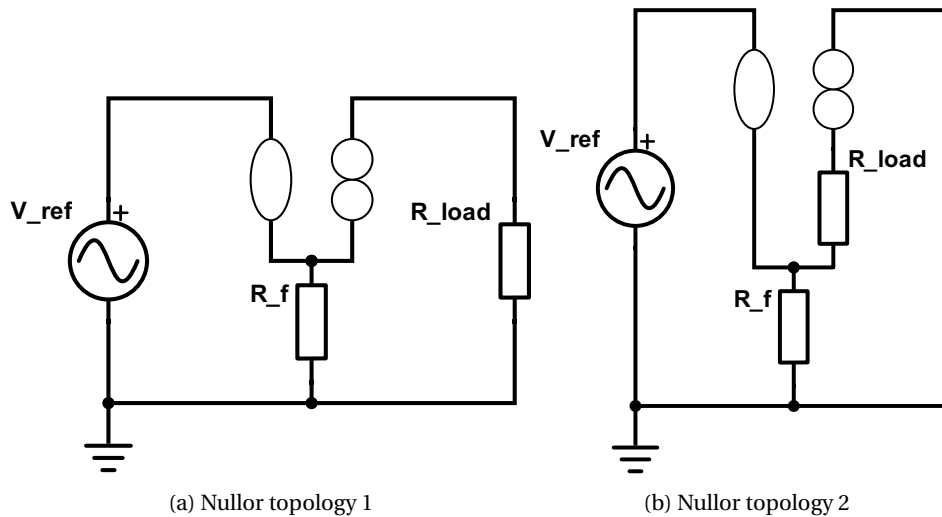


Figure 3.2: Transadmittance amplifier with a nullor

3.4.1. Transadmittance amplifier

Replacing the nullor in [Figure 3.2b](#) with an operational amplifier gives us the desired transadmittance amplifier, shown in [Figure 3.3](#). It has the following advantages and disadvantages:

Advantages

- + This circuit is relatively easy to implement, because only one resistor is needed (i.e. resistor R_f).

Disadvantages

- The output of the op-amp is directly connected to the load resistance. A high voltage operational amplifier is needed, which follows from requirement [R3](#).
- The op-amp has to supply a relatively large current of 100 mA according to requirement [R3](#).
- There are two undetermined nodes for the voltage measurement.
- R_f has to be accurate for a precise current according to [Equation 3.1](#). Also, resistance drift due to temperature variations should then be carefully analysed.

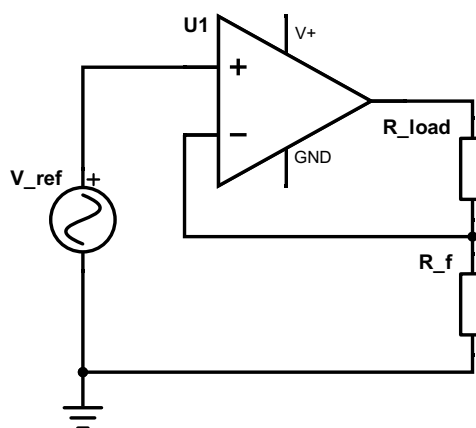


Figure 3.3: Transadmittance amplifier

There are not many op-amps that satisfy the requirement of high voltage and current. Therefore, the power to the load has to come from another source.

3.4.2. Transadmittance amplifier with a NPN transistor

In [Figure 3.4](#), the circuit is modified such that the power to the load is delivered by another source. In this circuit, the op-amp is used to control an NPN transistor. This solves the current requirement of the op-amp presented in the previous subsection. The circuit has the following advantages and disadvantages:

Advantages

- + The power to the heater is provided by another source.

Disadvantages

- A high voltage operational amplifier is needed, according to requirement [R3](#).
- There are two undetermined nodes for the voltage measurement.
- R_1 has to be accurate for a precise current according to [Equation 3.1](#). Also, resistance drift due to temperature variations should then be carefully considered.

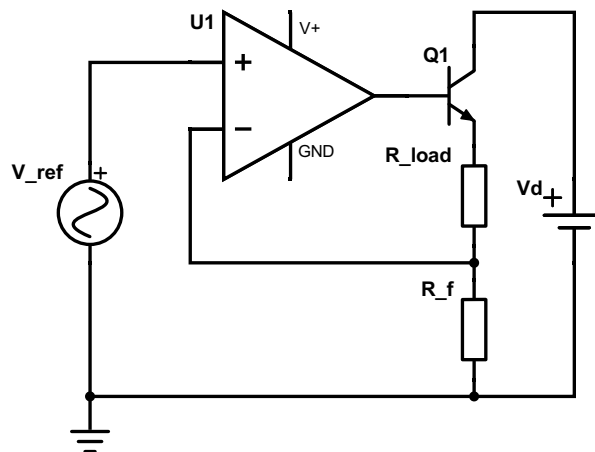


Figure 3.4: Transadmittance amplifier with NPN transistor

A high voltage op-amp is still needed. Therefore, the circuit has to be modified such that there is no need for a high voltage op-amp.

3.4.3. Transadmittance amplifier with a MOSFET

A third possibility is to move the load resistance out of the feedback loop and to replace the NPN transistor with a MOSFET. [Figure 3.5](#) shows the obtained circuit. The advantage of using a MOSFET instead of an NPN transistor is that the NPN transistor has an additional base current at the emitter. This means that the current through the load will be less than the current through R_f , which results in less precision by the current source. This effect is not as significant in a MOSFET and therefore, a MOSFET is used. This topology also makes this circuit a current sink instead of a current source. The advantages and disadvantages are:

Advantages

- + The power to the heater is provided by another source.
- + No high voltage op-amp is needed.
- + One undetermined node for voltage measurement, because we assumed V_d is accurate and known.

Disadvantages

- R_f has to be accurate for a precise current according to [Equation 3.1](#). Also, resistance drift due to temperature variations should then be carefully considered.

From the analysis above follows that the transadmittance amplifier with a MOSFET, as shown in [Figure 3.5](#), is the most convenient. The advantage that a low voltage operational amplifier can be used leaves us with more op-amps than we can choose from. Furthermore, the voltage read-out can be more accurate, as only one node is undetermined and the other is assumed to be known and accurate (as it comes from an accurate supply). Therefore, we will delve into the analysis of this configuration from now on.

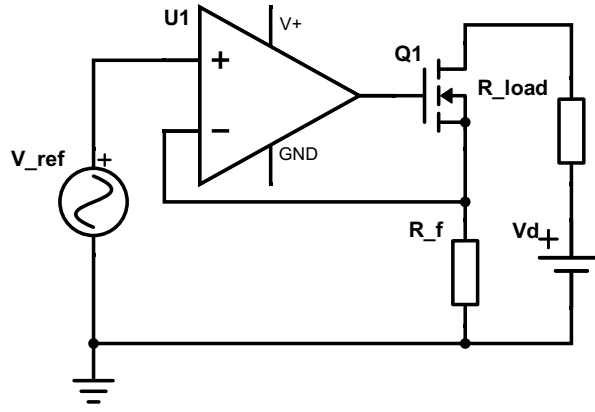


Figure 3.5: Transadmittance amplifier with MOSFET

3.5. Bandwidth analysis

The bandwidth of the system depends on the desired settling time of the system. In order to obtain an expression for the settling time, we assume that a first order system is acceptable for making an approximation. The transfer function of a first-order low-pass filter (one pole and no zeros) and a step response with magnitude V_{desired} is given by Equation 3.2 and Equation 3.3 respectively. The time constant is denoted by τ .

$$H(s) = \frac{1}{1 + s\tau} \quad (3.2)$$

$$s(t) = V_{\text{desired}} \left[1 - \exp\left(-\frac{t}{\tau}\right) \right] \quad (3.3)$$

The least significant bit (LSB) of the ADC specifies the smallest level that the ADC can convert. Equating the LSB to the difference in the desired steady state level and step response leads to Equation 3.4, with n the amount of bits of the ADC.

$$V_{\text{desired}} \cdot 2^{-n} = V_{\text{desired}} - V_{\text{desired}} \left(1 - \exp\left(-\frac{t}{\tau}\right) \right) \quad (3.4)$$

$$2^{-n} = \exp\left(-\frac{t}{\tau}\right) \quad (3.5)$$

$$n \ln(2) = \frac{t}{\tau} \quad (3.6)$$

$$\tau = \frac{t}{n \ln(2)} \quad (3.7)$$

The obtained expression can be rewritten to obtain the bandwidth by substituting Equation 3.8 in Equation 3.7 and solving for the bandwidth (B).

$$\tau = \frac{1}{2\pi B} \quad (3.8)$$

The obtained expression for the bandwidth is then given by Equation 3.9.

$$B_{\text{system}} = \frac{n \ln(2)}{2\pi t} \quad (3.9)$$

A 16-bit ADC is used, as explained by the readout subgroup [23]. According to requirement R6, the total delay from input to steady output is 24 μs . A settling time of 10 μs is chosen as requirement, which leaves enough

time for the output to respond to the input. Plugging these two numbers into Equation 3.9 gives us a show-stopper value for the bandwidth of the system. The obtained numeric result is 176508.48Hz. Taking 10% tolerance into account gives us the following show-stopper value for the bandwidth of the system:

$$B = 194\,159.33\text{Hz}$$

For a first-order low-pass filter, the effective noise bandwidth is higher than the calculated -3dB bandwidth. The relation between these two is given by Equation 3.10.

$$B_{\text{effective,noise}} = \frac{\pi}{2} B = 304\,984.76\text{Hz} \quad (3.10)$$

3.6. Feedback resistor analysis

3.6.1. Desired gain

A larger value of the feedback resistor will dissipate more power and thus generate more heat. The resistance changes with temperature according to Equation 3.11. Therefore, a smaller value for the feedback resistor is desired, since there will be less power dissipated in the resistor and in term the resistor will heat up less. Hence, the resistance value will drift less. Furthermore, the current through the load is related to the input voltage by the feedback resistor according to Equation 3.1. This means that a large feedback resistor will require a large input voltage in order supply a high current through the load to satisfy requirement R3. This input voltage is limited to the maximum voltage a pin of the microcontroller can supply.

$$R(T) = R_0(1 + \alpha\Delta T) \quad (3.11)$$

However, lower values of the feedback resistance means that deviations in the load current due to noise are increased. For example, a value of $1\,\Omega$ means that the input voltage range of the amplifier has to be between $0 - 100\text{ mV}$ (again, to comply with requirement R3). While this is possible, it means that noise will have a bigger impact. Also, resistances from the MOSFET and cables will have more influence with such a small feedback resistance.

Therefore, a trade-off is made and a value of $10\,\Omega$ was chosen. This means that the input voltage range of the op-amp has to be between $0 - 1\text{ V}$.

$$R_f = 10\,\Omega$$

3.6.2. Show-stopper values for the accuracy of the resistor

The transfer of the circuit, given by Equation 3.1, shows that the resistor in the feedback loop determines the transfer of the input voltage to the output current.

From requirement Sys 1, which states that the temperature must be controlled with an accuracy of $1\text{ }^\circ\text{C}$, it follows that the current source must be able to supply a current with an accuracy of $1\text{ }^\circ\text{C}$. The feedback resistor has two inherent practical limitations which can cause this requirement to not be satisfied; an offset in the resistance value and a nonzero temperature coefficient that causes resistance drift. The former is a constant offset, which causes a constant offset at the output. This can be compensated in the software. The latter, however, is temperature dependent and can affect the load current in such a way that a $1\text{ }^\circ\text{C}$ readout error is caused.

From [24], it followed that a $1\text{ }^\circ\text{C}$ change in temperature is read out by a $1.44\,\Omega$ change in resistance value of the load. This holds for a device with a resistance of $660\,\Omega$.

The value of the R_{load} is calculated by measuring the voltage across and current through the load and using $R_{\text{meas}} = \frac{V_{\text{meas}}}{I_{\text{meas}}}$ to calculate the resistance. This is also visualized in Figure 3.6. The current is measured by measuring the voltage over the feedback resistor and dividing it by the value of the feedback resistor. This

however does not involve the temperature drift of the resistor according to Equation 3.11. Therefore, there is a slight error in the measurement of R_{load} .

The maximum temperature drift of the feedback resistor can be calculated by using Equation 3.12. This equation is derived in Appendix C.

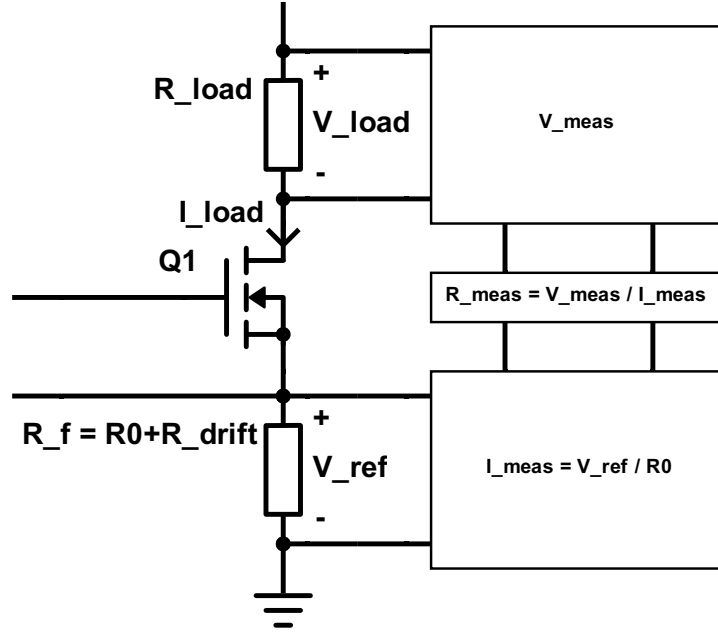


Figure 3.6: Load resistance calculation

$$R_{drift} = R_0 \left(\frac{R_{load}}{R_{load} + R_{error}} - 1 \right) \quad (3.12)$$

Plugging in a value of 10Ω for R_0 , 1000Ω for R_{load} according to specification S1 (the highest value is chosen because it gives the smallest acceptable R_{drift}) and 1.44Ω for R_{error} results in:

$$R_{drift, max} = 10 \left(\frac{1000}{1000 + 1.44} - 1 \right) = -0.0143379 \Omega$$

3.7. MOSFET analysis

3.7.1. MOSFET requirements

From requirement R3, it follows that I_{DS} has to be at least 100 mA and V_{DS} at least 70 V .

With a constant supply to the load, the MOSFET dissipates some power, which means there is a power requirement for the MOSFET. This power requirement can be calculated using Equation 3.13. The value for V_{ref} that will obtain the largest MOSFET power dissipation can be calculated using Equation 3.14. These formulas are derived in Appendix D.

Filling the values $V_d = 70 \text{ V}$, $R_{load} = 660 \Omega$ and $R_f = 10 \Omega$ gives a value of $V_{ref} = 0.5224 \text{ V}$ and thus the maximum power dissipation of the MOSFET is $P_{max} = 1.8284 \text{ W}$. Therefore, we decided with some margin that the requirement for the power dissipation of the MOSFET should be at least 2 W .

$$P_{MOSFET} = \left(V_d - R_{load} \frac{V_{ref}}{R_f} - V_{ref} \right) \frac{V_{ref}}{R_f} \quad (3.13)$$

$$V_{\text{ref}} = \frac{1}{2} \frac{V_d R_f}{R_{\text{load}} + R_f} \quad (3.14)$$

3.7.2. Modelling the MOSFET

Several efforts have been made in modelling a MOSFET [25]. LTSPICE also contains a library with MOSFET models and manufacturers of these devices also have their own model. However, working with these models would make the analysis, such as that of the gain-bandwidth product given in [Subsection 3.8.3](#), complex. In order to simplify the analysis while preserving the fundamental limitations, we will look at the simplified small-signal equivalent circuit for a MOSFET of which the source has been connected to the bulk [25]. Due to the physical structure of the device, the gate overlaps the diffusion area of the drain and source. This creates a capacitive effect, which explains the gate-drain and gate-source capacitances placed in the model. Furthermore, a capacitive effect exists between the drain and the source. These capacitances limit the frequency response of the circuit. At DC, these capacitances do not play a role. For a first model to determine the gain-bandwidth product, we will assume that our circuit is instantaneous and therefore neglect the capacitances.

Furthermore, the resistance R_{DS} can also be neglected for our purposes. The effect of this resistance is that the gate and drain voltages are lowered. To compensate for this, the op-amp will have to supply a bit more voltage to the gate to turn the device on. The reason for neglecting this resistance is that we are not power limited and are not interested in the power efficiency in this first prototype.

Therefore, the MOSFET model reduces to a voltage controlled current source. The nonlinearity of the MOSFET is preserved in the model, because the gain (g_m) of the VCCS is dependent on the drain source current as shown in [Equation 3.15](#).

$$g_m = \sqrt{\beta I_{\text{DS}}} \quad [\text{S}] \quad (3.15)$$

An approximation of β can be obtained by reading out a specific drain current at a specific gate source voltage from the I_{D} versus V_{GS} characteristic in the datasheet of the MOSFET. Then, by rewriting [Equation 3.16](#) into [Equation 3.17](#) and substituting the values, β is obtained.

$$I_{\text{DS}} = \beta (V_{\text{GS}} - V_{\text{T}})^2 \quad [\text{A}] \quad (3.16)$$

$$\beta = \frac{I_{\text{DS}}}{(V_{\text{GS}} - V_{\text{T}})^2} \quad \left[\frac{\text{A}^2}{\text{V}} \right] \quad (3.17)$$

3.8. Op-amp analysis

This section will present the analysis that leads to the show-stopper values for the op-amp. First, a show-stopper value for the noise is obtained in [Subsection 3.8.1](#). Then, [Subsection 3.8.2](#) briefly explains how the op-amp has been modelled. Lastly, [Subsection 3.8.3](#) presents the obtained show-stopper value for the gain-bandwidth product.

Besides these restrictions, the op-amp must have another important property. The input voltage range should be between 0 V and 1 V, because the DAC will provide the input signals within this range.

3.8.1. Noise analysis

As the value of the feedback resistor is now known, our next step is to obtain a show-stopper value for the noise of the operational amplifier. The software that we used were SLiCAP, MATLAB and LTspice. The nullor, shown in [Figure 3.2a](#), is an idealized circuit of the practical operational amplifier with MOSFET circuit, shown in [Figure 3.5](#). The working principle of the nullor can be regarded as a combination of an ideal op-amp and an ideal MOSFET in this specific case. This circuit, built in LTspice, is shown in [Figure 3.7](#). We have modelled the thermal noise generated by the resistors with a current source in parallel to the resistor [25]. Current source 'I3' represents the noise spectral density, $2qI_{\text{leakage}}$, associated with the leakage current of the MOSFET. Analyzing this circuit, we can reason that this leakage current has no effect. It is in parallel with the

norator. The norator will therefore compensate for this leakage current. Thus, the total load current remains the same. This conclusion also gives us insight in how the practical circuit of Figure 3.5 should operate. Here, the leakage current of the MOSFET is also compensated in the feedback loop.

The node 'out' and the node connected to the voltage supply 'V3' are the nodes used for the voltage readout. We assumed that V3 will be constant and accurate, thus the total noise at node 'out' is of interest. The maximum noise allowed at the load is 500 μV , as stated by requirement R5. Furthermore, a noise level restriction of 5 μV across the feedback resistance is set. The explanation can be found in [23]. This will be the second node of interest. Assuming the worst case scenario, i.e. a load of 1000 Ω , the equivalent maximum noise current through the load is 0.5 μA .

As explained, SLICAP is used to obtain the referred total noise spectral density at node 'out' and node 'feedback'. Integrating over the bandwidth gives the total equivalent noise at these nodes. At node 'out', the output quantity is the current and hence the total referred noise is expressed in Ampère. However, at node 'feedback', the output quantity is the voltage (which is also measured). Thus, the total referred noise is expressed in Volt. The symbolic expression for the total noise current referred to node 'out' and total noise voltage referred to node 'feedback' is given by Equation 3.18 and Equation 3.19 respectively. S_i and S_v are the current and voltage noise spectra respectively. The bandwidth of the system is denoted by B . The analysis above is also justified, as the leakage current of the MOSFET does not appear in this expression.

$$I_{nO} = \sqrt{B} \sqrt{\frac{S_v}{R_f^2} + \frac{4.0kT}{R_f} + \frac{S_i (R_f + R_s)^2}{R_f^2} + \frac{4kTR_s}{R_f^2}} \quad [\text{A}] \quad (3.18)$$

$$V_{n\text{Feedback}} = \sqrt{B} \sqrt{S_i R_s^2 + 4kTR_s + S_v} \quad [\text{V}] \quad (3.19)$$

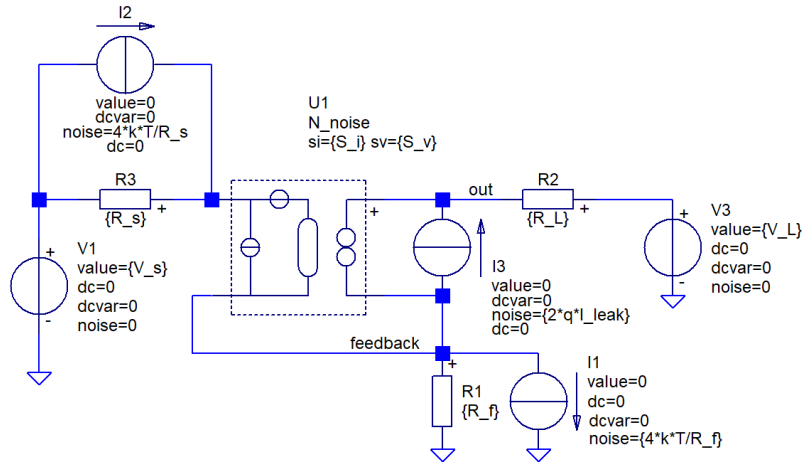


Figure 3.7: Circuit for noise analysis

To obtain a show-stopper value for the current noise spectrum of the operational amplifier, S_v is set to zero in Equation 3.18 and is equated to the maximum noise allowed at node 'out'. For the voltage noise spectrum the same holds except that now S_i is set to zero. The show-stopper values obtained are presented in Equation 3.20 and Equation 3.21. The minimum value is chosen in Equation 3.20, because it results in a stricter show-stopper value. As explained in the previous section, we have chosen the feedback resistance (R_f) to be 10 Ω . As follows from the heater specification S1, the load varies between 100 Ω and 1000 Ω . To obtain worst-case show-stopper values, we have taken R_L to be 1000 Ω . The estimated equivalent noise bandwidth of the system, as explained in Section 3.5, is substituted for B and we assumed that the operating condition is at room temperature.

$$S_v = \min \left\{ \left(\frac{(R_f I_{nO})^2}{B} - 4kT(R_f + R_s) \right), \left(\frac{V_{nFeedback}^2}{B} - 4kT R_s \right) \right\} = 8.1809 \cdot 10^{-17} \text{ V}^2/\text{Hz} \quad (3.20)$$

$$S_i = \min \left\{ \left(\frac{1}{B} \left(\frac{R_f I_{nO}}{R_f R_s} \right)^2 - \frac{4kT}{R_f + R_s} \right), \left(\frac{V_{nFeedback}^2}{R_s^2 B} - \frac{4kT}{R_s} \right) \right\} = 8.1564 \cdot 10^{-19} \text{ A}^2/\text{Hz} \quad (3.21)$$

3.8.2. Modelling the operational amplifier

We have modelled the op-amp as a VCVS with an output resistance. We have not modelled the common mode and differential mode input resistance and capacitance of the operational amplifier, as this would make the analysis of the gain-bandwidth product more complicated. The op-amp is modelled as a first-order low pass system with a DC gain (A_0). The transfer is given by Equation 3.22. Factor GB is the gain-bandwidth product.

$$G = \frac{A_0}{1 + s \frac{A_0}{2\pi GB}} \quad (3.22)$$

3.8.3. Gain-bandwidth analysis

The next step in the design is to obtain a show-stopper value for the gain-bandwidth product of the operational amplifier. For this step, we must replace the nullor of circuit Figure 3.7 and place a model of the MOSFET in the circuit. First, we will elaborate the models chosen for the op-amp and MOSFET. Next, the circuit schematic is presented. Lastly, the obtained show-stopper value for the gain-bandwidth product is presented and discussed.

SLICAP is used to obtain a show-stopper value for the gain-bandwidth product of the op-amp. The script is based on the code in [25]. First, the order of the loop gain is calculated. Then, an expression for loop gain-poles product is obtained. By equating the desired bandwidth with the bandwidth following from the loop gain-poles product and solving for the gain-bandwidth product Equation 3.23 is obtained.

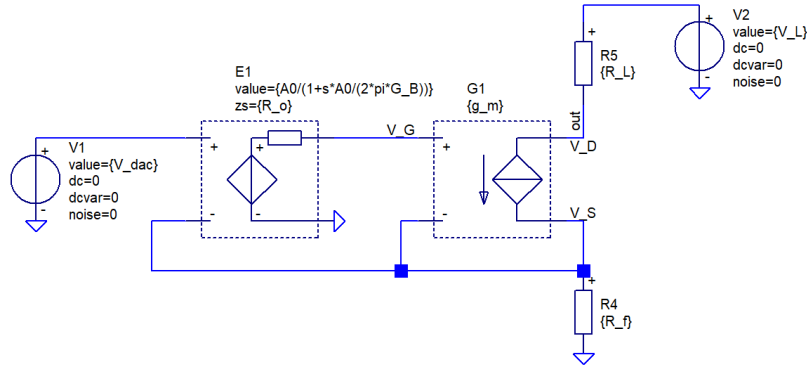


Figure 3.8: Circuit for analysing the gain-bandwidth product

$$GB_{\min} = \frac{0.3183\pi B (R_f g_m + 1.0)}{R_f g_m} \quad [\text{Hz}] \quad (3.23)$$

In the design phase, the components are not yet chosen. Therefore, the numeric result will be given in Chapter 4 when a suitable MOSFET has been presented.

Note that if the drain-source current goes to zero, g_m drops to zero according to Equation 3.15. This would result in an infinite gain-bandwidth product. Thus, one of the consequences of choosing this current source topology is that the drain-source current cannot drop to zero. Also, a very low current would require a very

large gain-bandwidth product. Thus, the result is that the power efficiency of the system is lower and a higher current value should be used for measurements. We assume that a higher measurement current will not heat up the device up to a level such that it has a detrimental effect for the measurements. The reason for this is because the duration of the (measurement) pulse is very short, as can be read in Section 3.9. Furthermore, power efficiency is not a main concern.

3.9. System measurement method

Figure 3.9 visualizes the variation between measuring the temperature of the device and heating up the device. During certain time instances, the device is heated up as shown by the larger values of current. Then, for a short time interval, a short pulse is sent through the device. The duration of the pulse should be long enough in order for the measurement signal to settle (within 1 LSB) to the desired level. But, on the other hand, it should be as short as possible, such that the measurement pulse will not affect the temperature read-out.

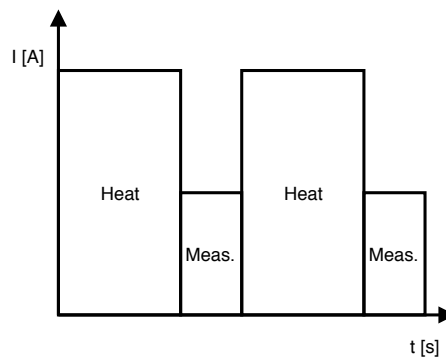


Figure 3.9: Measurement method of the whole system

3.10. Component requirements

The requirements for the components that follow from the derived show-stopper values and program of requirements are summarized below.

3.10.1. Circuit requirement

- C1 Bandwidth > 200 kHz

3.10.2. Op-amp requirements

We have assumed that a nonzero input offset voltage and current can be compensated in the software, as this is a constant error.

- O1 $S_v < 8.1809 \cdot 10^{-17} \text{ V}^2/\text{Hz}$
- O2 $S_i < 8.1564 \cdot 10^{-19} \text{ A}^2/\text{Hz}$
- O3 Gain-bandwidth product > $\frac{0.3183\pi B(R_f g_m + 1.0)}{R_f g_m} \text{ Hz}$
- O4 Supply voltage > V_T
- O5 Input range between 0 V and 1 V

3.10.3. MOSFET requirements

Below are the main requirements for the MOSFET shown. These are the minimal functional requirements. At higher drain-source currents or voltages, the capacitances inherent to the MOSFET are becoming generally larger. The value of these capacitances are found in the datasheet of the MOSFETs and depend on the frequency. A lot of MOSFETs can be found with the presented requirements. To help us make a better decision, we set up desired specifications. These specifications are not exactly determined and therefore called 'desired'. By choosing the threshold voltage of the device relatively lower, the gate voltage can be less. If the device has low parasitic capacitances, the delay introduced in this device is reduced. This is closely related to the rise time, turn-on delay time and fall time of the device. Hence, the desired specifications are used to choose from the MOSFETs which comply with the main requirements (M1, M2 and M3).

M1 $I_{DS} > 100 \text{ mA}$

M2 $V_{DS} > 70 \text{ V}$

M3 Power rating $> 2 \text{ W}$

3.10.4. MOSFET desired specifications

MD1 V_T as low as possible

MD2 Parasitic capacitances as low as possible

MD3 Rise time as low as possible

MD4 Turn-on delay time as low as possible

MD5 Fall time as low as possible

3.10.5. Feedback resistor requirements

F1 Resistance value = 10Ω

F2 Resistance drift due to temperature $|R_{\text{drift}}| < 0.0143379 \Omega$

F3 Power rating $> 0.1 \text{ W}$

4

Implementation

In this chapter we will discuss the chosen components. First, we will justify the choice for feedback resistor in [Section 4.1](#), then the MOSFET in [Section 4.2](#) and lastly, the op-amp in [Section 4.3](#). Furthermore, we will characterise certain parameters of these devices, because the datasheet only shows typical values and often different test conditions. In [Section 4.4](#) we will present the prototype.

4.1. Implementation of the feedback resistor

According to requirement [F1](#) and [F2](#) the feedback resistor must have a value of $10\ \Omega$ and a maximum temperature drift $|R_{\text{drift}}| < 0.0143379\ \Omega$. Furthermore, the resistance should be able to dissipate at least $0.1\ \text{W}$.

We have chosen for the WSC251510R00FEA surface mount wirewound resistor. The main advantage of this SMD resistor is that it can handle $3\ \text{W}$. We have chosen for an SMD resistor, because we want to implement the circuit on a PCB.

The resistance drift due to temperature is $50\ \text{ppm}/^\circ\text{C}$. For a $10\ \Omega$ resistance value, this translates to a drift of $5 \cdot 10^{-4}\ \Omega/^\circ\text{C}$. Therefore, the maximum temperature variation that is permitted is $\frac{0.0143379}{5 \cdot 10^{-4}} = 28\ ^\circ\text{C}$. We assume that a maximum power dissipation of $0.1\ \text{W}$, as explained in the previous chapter, will not cause temperature variations of more than $28\ ^\circ\text{C}$. Therefore requirement [F2](#) is satisfied. Furthermore, wirewound resistors tend to be cheaper than metal-foil type resistors, while still having good performance parameters [\[15\]](#).

Table 4.1: Requirements for the feedback resistor

Design	Requirement	Actual value
F1 Resistance value	$10\ \Omega$	$10.0\ \Omega$
F2 Resistance drift due to temperature	$0.0143379\ \Omega$	$50\ \text{ppm}/^\circ\text{C} \Rightarrow \text{max. } \pm 28\ ^\circ\text{C deviation}$
F3 Power rating	$0.1\ \text{W}$	$3\ \text{W}$

4.2. Choice of MOSFET

The MOSFET which we have chosen is the STP3N80K5 power MOSFET. Because a lot of power gets dissipated and a high drain voltage must be handled, a power MOSFET was needed. Despite the relatively high drain source voltage, the parasitic capacitances were relatively low. [Table 4.2](#) summarizes the requirements.

Table 4.2: Requirements for the MOSFET

Design	Requirement	Actual value
M1 I_{DS}	100 mA	2.5 A
M2 V_{DS}	100 V	800 V
M3 Power rating	2 W	60 W

4.3. Choice of op-amp

The op-amp complying with the requirements specified in Subsection 3.10.2 is the Linear Technology LT6203CS8#PBF. In order to obtain a show-stopper value for the gain-bandwidth product with Equation 3.23, the datasheet of the MOSFET was consulted. The maximum current to be supplied is 0.1 A. We would like to know what the required gate source voltage is to achieve this current. For this, we looked at the I_D vs V_{GS} graph in the datasheet. Because we had to choose a power MOSFET, the graph cannot be accurately read-out at low drain currents. Furthermore, the graph presented was only valid for a certain drain source voltage over the MOSFET. Therefore, the best we could do is to obtain an approximation. At a I_{DS} of 0.1 A, a V_{GS} of 5.6 V is read-out and, assuming the worst-case threshold voltage, the transconductance is found to be 0.28 S. Now, substituting the values in Equation 3.23 leads to the gain-bandwidth product presented below.

Table 4.3: Requirements for the op-amp

Design	Requirement	Actual value
O1 Input noise voltage spectral density	$8.1809 \cdot 10^{-17} \text{ V}^2/\text{Hz}$	$3.61 \cdot 10^{-18} \text{ V}^2/\text{Hz}$
O2 Input noise current spectral density	$8.1564 \cdot 10^{-19} \text{ A}^2/\text{Hz}$	$1.21 \cdot 10^{-24} \text{ A}^2/\text{Hz}$
O3 Gain-bandwidth product	265 kHz	90 MHz
O4 Supply voltage	$> V_T = 5 \text{ V}$	2.5 V to 12.6 V
O5 Input voltage range	0 V - 1 V	Rail-to-rail input

4.4. Prototype

The obtained circuit is soldered on a breadboard, as shown in Figure 4.1b. One thing to notice is that we have placed bypass capacitors at the input of the op-amp and parallel to the supply voltage to the load. This is common practice which reduces the voltage ripple. The circuit has also been designed on a PCB. However, due to a larger than expected delivery time, the circuit has not been soldered yet.

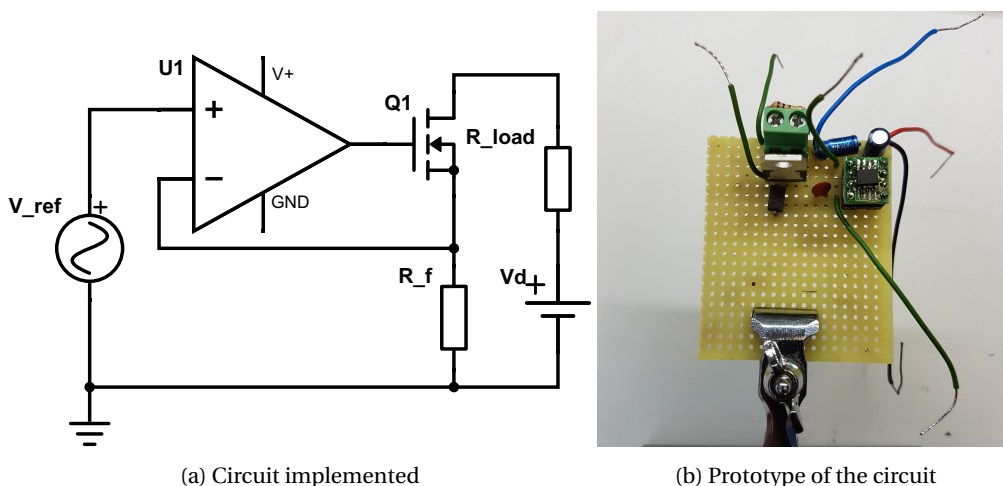


Figure 4.1: Prototype

5

Evaluation

In this chapter we will explain how we have verified the performance of the prototype. We will start by giving an overview of the test plan and summarize the design requirements in [Section 5.1](#). Then, we evaluate each design requirement in [Section 5.2](#).

5.1. Overview

We have distinguished three different test methods. The first test is a noise calculation. In the second test, we have tested the current source separately. To do this, the control system and DAC are replaced by a PWS4205 programmable DC power supply and the microthruster is replaced by a generic resistor. Furthermore, the supply to the op-amp is also regulated by another DC power supply of the same type. In order to measure the current through the load, a Keithley 2450 SourceMeter supply is used. For the third method, we have integrated the components presented in [\[23\]](#) and [\[24\]](#) and tested the system on a microthruster. The parameter of interest is the deviation of the measured current and the desired current set by the control system. [Table 5.1](#) summarizes the requirements for the supply from [Chapter 2](#) and lists the section where the requirement is tested.

For the supply to the op-amp and load resistance, as shown in [Figure 5.1](#), a constant voltage is chosen. For the positive input of the op-amp, a square wave is used. The reason is because it represents the output of the digital-to-analog converter the best, as it would also switch (i.e. step) between certain voltage levels. Each subsection will now explain how the output is measured.

Table 5.1: Requirements and the sections where the requirements are tested

Requirement	Section
R1 The supply has to deliver a frequency signal	Subsection 5.2.3
R2 The supply has to be controlled with a voltage signal	Subsection 5.2.2
R3 Heating current of 100 mA through the load	Subsection 5.2.2
R4 Sensing current of 50 mA through the load	Subsection 5.2.2
R5 Maximum equivalent noise voltage of 500 μ V over the load	Subsection 5.2.1
R6 During sensing (i.e. when a current of 50 mA is supplied), the time between a change in the input of the system and the output settling to 1 LSB should be less than 34 μ s	Subsection 5.2.3 - Subsection 5.2.4
R7 Influence of variations in load resistance on the output current should be minimized	Subsection 5.2.2

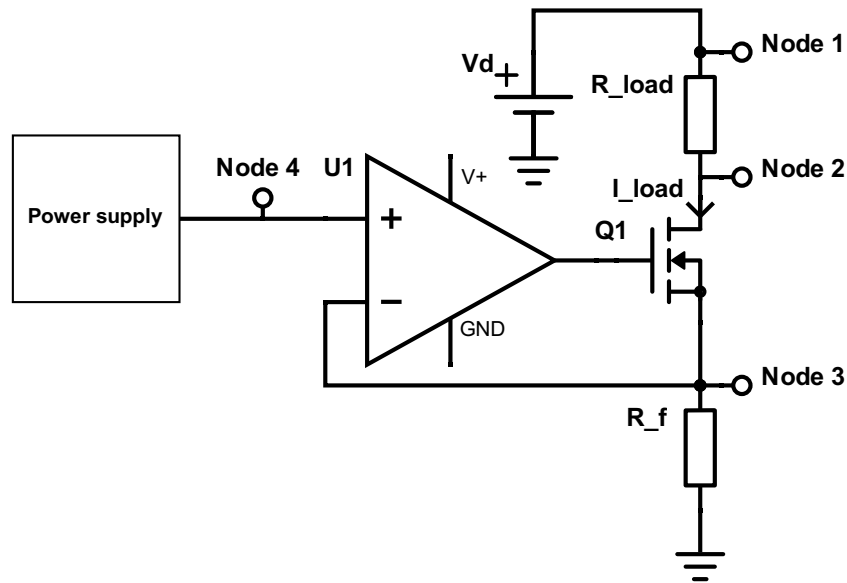


Figure 5.1: Circuit for measurements

5.2. Testing and results

We tested the circuit by connecting a function generator at the input of the op-amp. A generic resistor is used as load.

5.2.1. Noise

The parameters for the noise voltage and current spectral density in the simplified noise current expression obtained in [Subsection 3.8.1](#) are substituted. The allowed noise current through the load and noise voltage over the feedback resistance are $5 \cdot 10^{-7}$ A and $50 \cdot 10^{-7}$ V.

As expected, the noise requirements are met. However, the noise expressions obtained in [Subsection 3.8.1](#) are based from simplified models. We must realise that the input resistance of the op-amp is not infinite and that the MOSFET will also contribute to the noise. The equivalent noise current through a load of 1000Ω and the equivalent noise voltage across the feedback resistance are given by [Equation 5.1](#) and [Equation 5.2](#) respectively.

$$I_{nO} = 1.0726 \cdot 10^{-7} \text{ A} \quad (5.1)$$

$$V_{n\text{Feedback}} = 1.0725 \cdot 10^{-7} \text{ V} \quad (5.2)$$

5.2.2. Accuracy of the circuit

Accuracy with different inputs

The accuracy of the circuit is tested by using a programmable power supply at the input of the op-amp with voltages ranging from 0.1 V to 1 V, which meets requirement [R2](#). The Keithley source meter is used as V_d and also to measure to the current through the load by connecting the sense probes of the Keithley to 'Node 1' and 'Node 2' of [Figure 5.1](#). A generic load resistor of 99.3Ω is used as load. This specific value for the resistance was chosen, because then the circuit can be tested from 0 mA to 100 mA without the need for higher voltages than 20 V. The results are shown in [Figure 5.2a](#), together with the theoretical values. The resistance of the feedback resistor is measured with a digimess RLC 200: Programmable automatic RLC meter and found to be 10.0Ω . The theoretical value for the current is calculated by dividing the supplied voltage at the input of the op-amp by the value of the feedback resistance.

To better analyse the deviation from the ideal values, the ideal values are subtracted from the measured values. The results can be found in [Figure 5.2b](#). The figure shows that there is a small offset of approximately 0.26 mA. Possible reasons for this could be that the MOSFET can not switch fast enough and the nonzero input offset voltage drift of the op-amp. This offset can be compensated in software. The variance of the deviation is approximately 0.08 mA. The noise requirement [R5](#) stated that a maximum noise of 500 μV is allowed for full resolution of the ADC. This translates to an equivalent noise current of 5 μA . If we would compare these two figures, it would mean that we have 16 times more noise on the output than allowed. However, to obtain a more reliable number for the variance, more measurements should be performed. Furthermore, the output of the power supply and the use of lengthy cables also introduce noise in the system. Therefore, the exact noise generated within the current source circuit is not determined with this method, but rather an approximation of the total noise is given. However, this requirement was set very strict. Controlling and reading out the temperature can still be achieved and an integrated test (i.e. with the results from the thesis [\[24\]](#) and [\[23\]](#)) should be performed to verify this.

As the figures show, a sensing current of 50 μA and a heating current of 100 μA can be delivered. Therefore, requirements [R3](#) and [R4](#) are also satisfied.

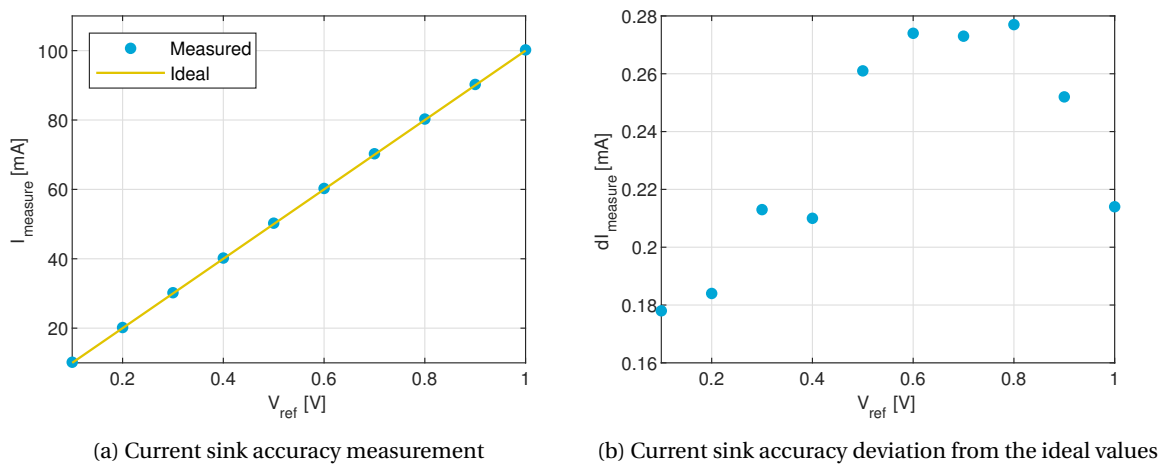


Figure 5.2: Results from the accuracy measurement of the current sink

Accuracy with varying load

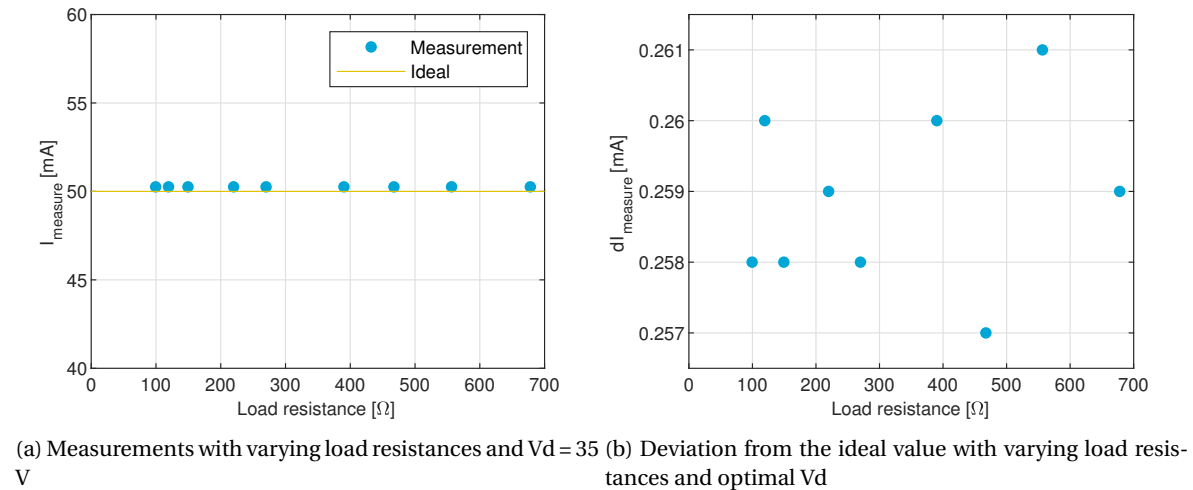
With the same measurement setup as explained in the previous subsection, the measurements with a varying load are carried out. Here the load resistor is varied from 100 Ω to 680 Ω and the current through the load is measured. A higher load resistance could not be tested, because it would exceed the safety limit. An input voltage of 500 mV is used and the Keithley is set to supply 35 V at V_d . The results are shown in [Figure 5.3a](#) and the deviation from the ideal values is shown in [Figure 5.3b](#).

It can be seen there is an offset of about 0.259 mA and a variation of about 0.002 mA. We observed that when we applied compressed air to cool down the op-amp, the offset changed. Therefore, this offset is probably caused by the nonzero input offset voltage drift of the op-amp. When we applied the compressed air to cool down the feedback resistance, nothing happened. Therefore, we can conclude that the temperature variation in the feedback resistance does not influence the measurements.

To conclude, the supplied current through the load is irrespective of the load and requirement [R7](#) is satisfied.

5.2.3. Maximum response time of 24 μs when sense current is supplied

The maximum response time is measured by applying a square wave with a high of 500 mV and a low of 0 mV. The frequency of the signal is 200 kHz from requirement [C1](#). The measurements are done with a Tektronix TDS2022C oscilloscope with channel 1 at 'Node 2' and channel 2 at 'Node 4' in [Figure 5.1](#).

Figure 5.3: Results from the measurements with varying loads and $V_d = 35$ V

The obtained measurement is given by Figure 5.4. It is found that the system had a response time of 33.6 ns. Or in other words, when a step at the input of the op-amp is applied, the output voltage at the load needed 33.6 ns to respond accordingly.

The response time is influenced by several factors. The op-amp and MOSFET impose a delay on the system. Furthermore, we have not incorporated the delay imposed by the DAC. The datasheet of the DAC tells us that it should have a response time of 4 μs . Because we have 33.967 μs margin left to still satisfy requirement R6, we can assume that the system with the DAC will be fast enough. Therefore, we can conclude that requirement R6 has been met if the settling time is less than 33.967 μs . From this measurements it can also be seen that the supply can deliver a frequency signal (in the form of a pulse), thus requirement R1 is met.

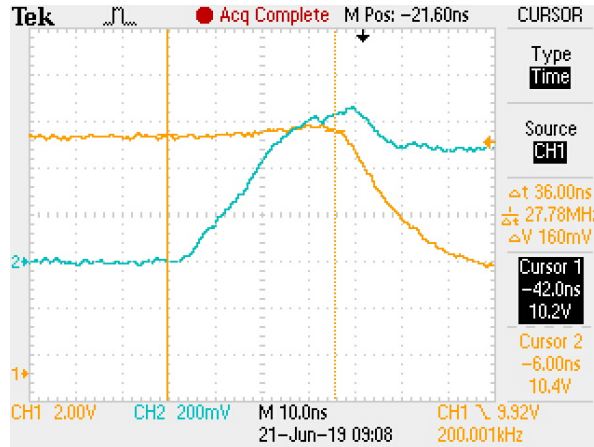


Figure 5.4: Response time measurement with 50mA and 300kHz

5.2.4. Maximum settling time of 10 μs

For the measurement of the settling time we again used the function generator at the input. Channel 1 of the oscilloscope is measured at 'node 3' in Figure 5.1. Two square waves with different amplitudes but the same frequency of 200 kHz (which is the required bandwidth of the circuit, as stated by requirement C1) are tested. One with a low of 0 mV and a high of 500 mV and one with a low of 0mV and a high of 1000 mV. The reason for these input levels is that these correspond to the desired sense and heat current respectively. Figure 5.5a and Figure 5.5b show the obtained response for the two input levels respectively.

The obtained results are presented in Table 5.2. We can conclude that requirement R6 has been met. The

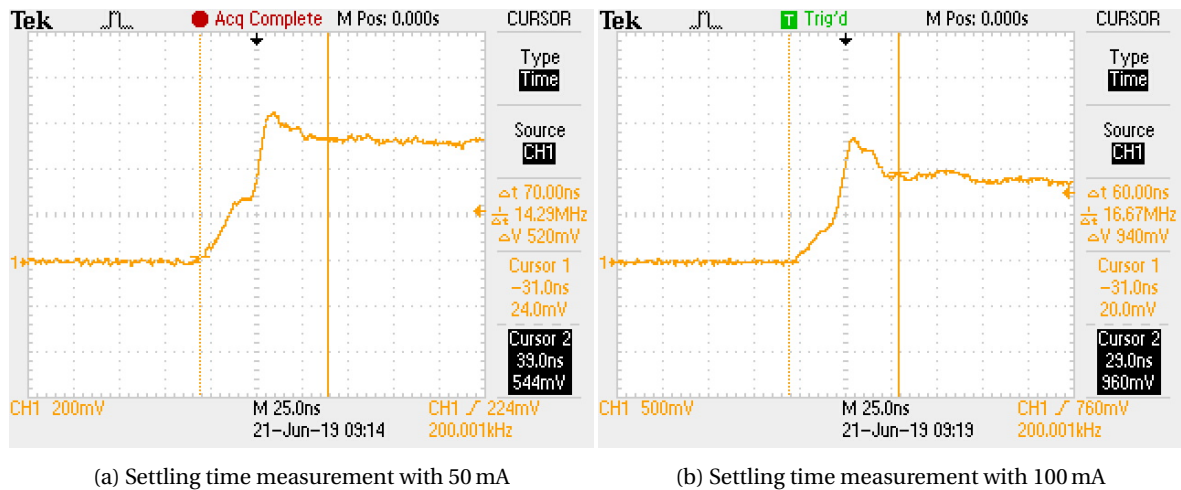


Figure 5.5: Settling time measurements

assumption was made that the influence of the ADC on the settling time of the system can be neglected. Because we have $33.897\ \mu\text{s}$ and $33.907\ \mu\text{s}$ margin, we assume that this assumption is valid. However, one thing to notice is that we could not read out the settling time within 1 LSB of the desired value. Our measurement equipment was not suited for this. Instead, we approximated it by taking the settling time longer on purpose. Despite this, a lot of margin is left and thus, the requirement is reached.

Table 5.2: Comparison between the target and measured values

Target value	Measured value at 500 mV	Measured value at 1000 mV
$10\ \mu\text{s}$	$0.070\ \mu\text{s}$	$0.060\ \mu\text{s}$

5.3. System integration

The control unit, read-out circuitry and the current source were integrated and tests were performed. An overview of the system is given in [24]. The results are shown in Figure 5.6. Figure 5.6a visualizes the supplied current and the measured current. The supplied current is the current desired by the control unit. As explained before, it is given in the form of a voltage as input to the current source. The measurement current is the current measured through the feedback resistance. The figure shows that the supplied current is increased linearly from 0 mA to 15 mA. Figure 5.6b shows the difference between the supplied current and the measured current. A negative slope in time is observed. The reason for this is not clear. However, we can see that the deviation is in the order of $+2 \cdot 10^{-4}$ A to $-3.5 \cdot 10^{-4}$ A. The requirement was that a deviation in the order of 10^{-6} A was allowed. Therefore, we can conclude that the system is not as accurate as desired. This can be due to several reasons. The deviation of the current source when measured separated from the complete system was found to be approximately $1.5 \cdot 10^{-4}$ A. Therefore, additional noise is also introduced in the read-out circuitry and digital-to-analog converter.

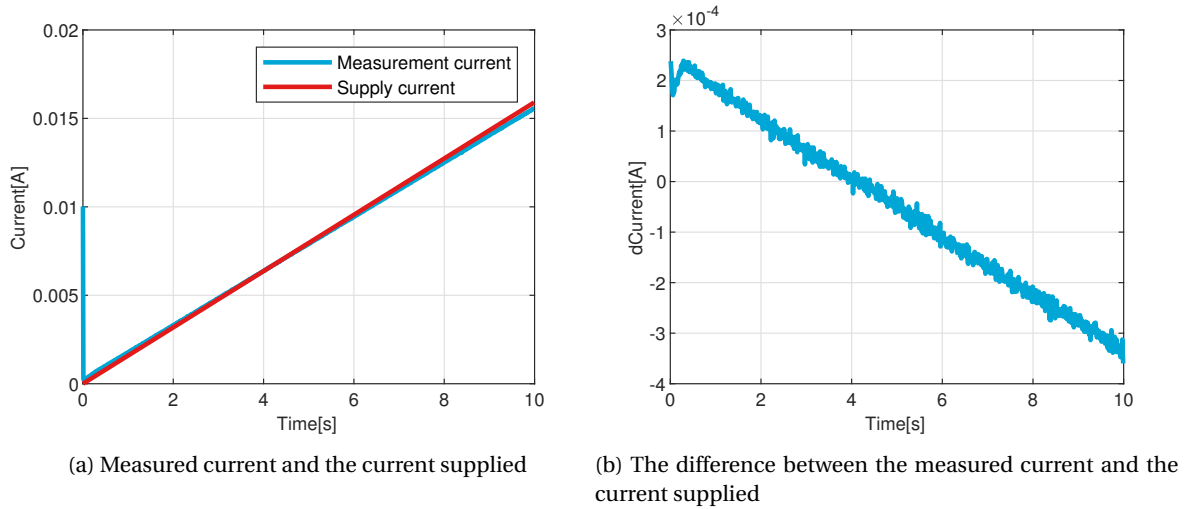


Figure 5.6: System integration measurements

5.4. Assessment

Table 5.3 summarizes the requirements. As can be seen, requirement R5 has not been met. The noise measured was in the order of 16 times more than stated by the requirement. However, this was expected. The requirement was set very strict, because it is not known whether a 1°C read-out accuracy is needed to control the temperature within 10°C . Thus, the presented prototype for controlling the temperature should be tested on a device with propellant and a thermal camera should be used to verify if the temperature stays within 10°C .

Table 5.3: Requirements results

Requirement	Achieved
R1 The supply has to deliver a frequency signal	✓
R2 The supply has to be controlled with a voltage signal	✓
R3 Heating current of 100 mA through the load	✓
R4 Sensing current of 50 mA through the load	✓
R5 Maximum equivalent noise voltage of $500 \mu\text{V}$ over the load	✗
R6 During sensing (i.e. when a current of 50 mA) is supplied, the time between a change in the input of the system and the output settling to 1 LSB should be less than $34 \mu\text{s}$	✓
R7 Influence of variations in load resistance on the output current should be minimized	✓

6

Conclusion

The two main objectives of this project were to study the dynamic liquid vapor phenomenon by acquiring data about the temperature of the heating element and to control the temperature of the heating element in an effort to reduce bubble forming. This report presented the design and implementation of a current source. It is used to heat and measure the resistive element of the microthruster and thus, it is a vital component in the system.

The source has been tested separately, which showed that the requirements for the delay between a change in the input and the output settling are met. However, the accuracy deviation at the load was approximately 16 times more than allowed. The source of this error has to be investigated further. The measurement equipment, i.e. the DC power supply and Keithley, also contribute to this error. Therefore, the measurement setup has to be reconsidered such that the influence on the total noise by these measurement equipment is diminished. Furthermore, we used lengthy cables for the measurements, which also introduce noise to the system. Accurately measuring the inaccuracies on microscale is thus a future challenge. But, beforehand it was known that this accuracy requirement, i.e. requirement R5, was set extremely strict for the reason that the behaviour and characteristics of the device were not known. Despite not reaching this requirement, the temperature of the device could still be controlled and read-out accurately. Therefore, tests should be performed in the future on a microthruster device with the read-out circuitry and control algorithm in software integrated to see if the temperature can be regulated within 10 °C.

The source has been integrated with the digital-to-analog converter, read-out circuitry and control unit. Tests were performed on a microthruster without propellant which showed that the demanded current (set by the control unit) deviated from the measured current (i.e. the current delivered by our system). Again, several factors contribute to this deviation, such as the read-out circuitry and cables. Therefore, the functional requirement Sys 1 was not met. However, the first objective of the complete project, i.e. to acquire data about the temperature of the device, is accomplished and the second objective, i.e. to control the temperature of the device, also, which can be read in [23] and [24]. Therefore, it can be concluded that the presented current source is adequate.

6.1. Future work

There are a number of improvements which can be made. These are listed below.

- Because the accuracy requirement R5 was set very strict, further tests should be performed to see whether a stable and accurate (i.e. within 10 °C range from a set-point) temperature control is achieved with the supply. If this is the case, we have met the goal to control the temperature of the resistance despite boiling phenomena and therefore, the current source is adequate.
- A buck-boost converter should be used to supply the load based on the current demanded by the control unit, instead of supplying maximum voltage to the load. This improves the efficiency.
- Shorter and better (i.e. with less noise) cables should be used in order to diminish the noise introduced.

- More measurements should be performed to characterise the current source. Also, a thermal camera should be used to validate if the temperature of the device read out is the same as the temperature given by the thermal camera. In that way, the requirement of having 1 °C (Sys 1) read-out accuracy could be tested.
- Supplying higher voltages than 40 V to the load should be done in order to test the functionality of the source at load resistance of above 100 Ω .
- The circuit should be built on the PCB and tested.
- Space phenomena should be studied and accounted for in the design, in order to make the system work in space.

A

Microthruster

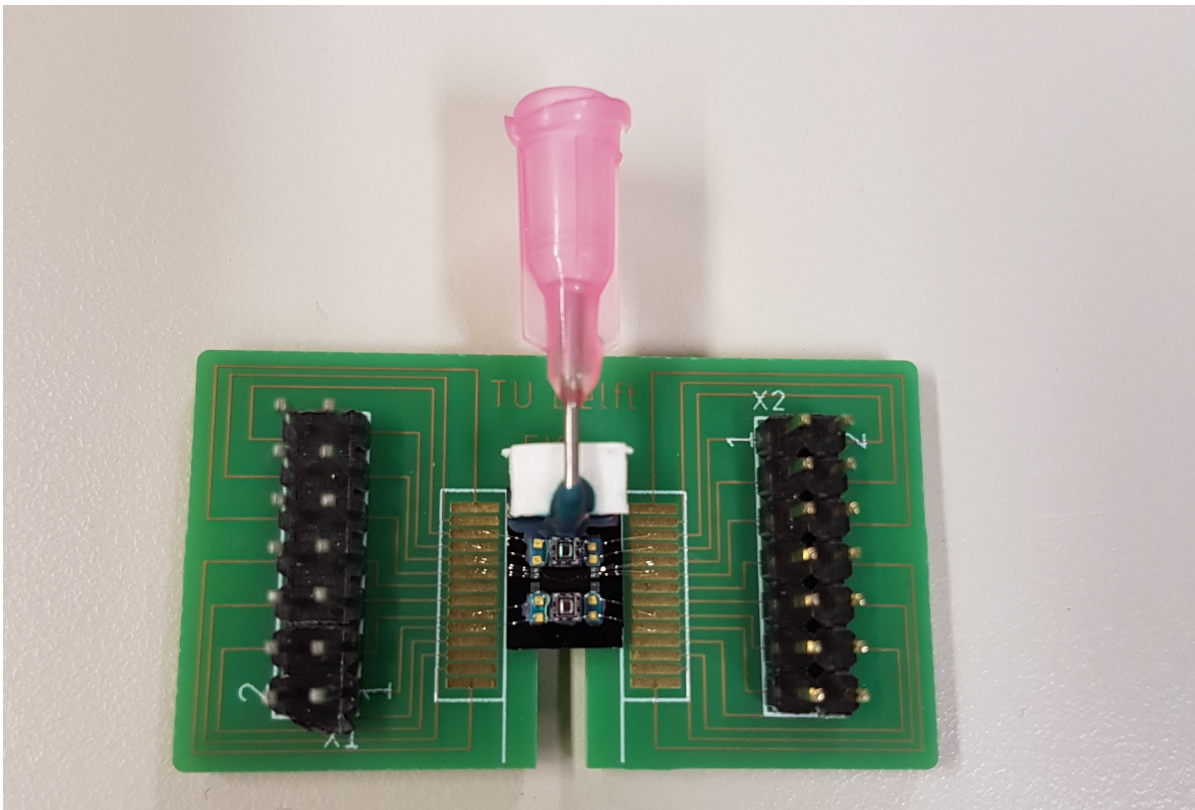


Figure A.1: VLM microthruster with pressure sensors

B

Component list

Table B.1: Components used for current sink

Component	Type	Datasheet link
Op-amp	LT6203CS8#PBF	https://www.analog.com/media/en/technical-documentation/data-sheets/620234fd.pdf
MOSFET	STP3N80K5	https://www.st.com/resource/en/datasheet/stf3n80k5.pdf
Resistor	WSC251510R00FEA	https://www.vishay.com/docs/30102/wscwsn.pdf
DAC	AD5061BRJZ-2500RL7	https://www.analog.com/media/en/technical-documentation/data-sheets/AD5061.pdf

C

Derivation the maximum feedback resistor drift

Equation C.12 is derived by as follows. The measurement error of load resistor R_{error} is calculated using Equation C.5. Substituting Equation C.4 and then Equation C.2 and Equation C.3 give Equation C.7. After rearranging the equation, the formula becomes Equation C.12.

$$I_{\text{load}} = \frac{V_{\text{ref}}}{R_f} = \frac{V_{\text{ref}}}{R_0 + R_{\text{drift}}} \quad (\text{C.1})$$

$$V_{\text{meas}} = V_{\text{load}} = I_{\text{load}} R_{\text{load}} = \frac{V_{\text{ref}}}{R_0 + R_{\text{drift}}} R_{\text{load}} \quad (\text{C.2})$$

$$I_{\text{meas}} = \frac{V_{\text{ref}}}{R_0} \quad (\text{C.3})$$

$$R_{\text{meas}} = \frac{V_{\text{meas}}}{I_{\text{meas}}} \quad (\text{C.4})$$

$$R_{\text{error}} = R_{\text{meas}} - R_{\text{load}} \quad (\text{C.5})$$

$$= \frac{V_{\text{meas}}}{I_{\text{meas}}} - R_{\text{load}} \quad (\text{C.6})$$

$$= \frac{\frac{V_{\text{ref}}}{R_0 + R_{\text{drift}}} R_{\text{load}}}{\frac{V_{\text{ref}}}{R_0}} - R_{\text{load}} \quad (\text{C.7})$$

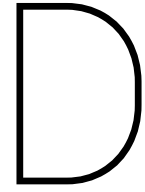
$$= \frac{R_0 R_{\text{load}}}{R_0 + R_{\text{drift}}} - R_{\text{load}} \quad (\text{C.8})$$

$$R_{\text{load}} + R_{\text{error}} = \frac{R_0 R_{\text{load}}}{R_0 + R_{\text{drift}}} \quad (\text{C.9})$$

$$R_0 + R_{\text{drift}} = \frac{R_0 R_{\text{load}}}{R_{\text{load}} + R_{\text{error}}} \quad (\text{C.10})$$

$$R_{\text{drift}} = \frac{R_0 R_{\text{load}}}{R_{\text{load}} + R_{\text{error}}} - R_0 \quad (\text{C.11})$$

$$R_{\text{drift}} = \left(\frac{R_{\text{load}}}{R_{\text{load}} + R_{\text{error}}} - 1 \right) R_0 \quad (\text{C.12})$$



MOSFET nodal analysis

With nodal analysis we can write V_d in terms of V_{load} , V_{DS} and V_{ref} .

$$V_d = V_{load} + V_{DS} + V_{ref} \quad (D.1)$$

Rearranging the equation gives [Equation D.3](#).

$$V_{DS} = V_d - V_{load} - V_{ref} \quad (D.2)$$

$$= V_d - R_{load} \frac{V_{ref}}{R_f} - V_{ref} \quad (D.3)$$

The power to the MOSFET can be calculated using [Equation D.5](#).

$$P_{MOSFET} = V_{DS} I_{load} \quad (D.4)$$

$$= \left(V_d - R_{load} \frac{V_{ref}}{R_f} - V_{ref} \right) \frac{V_{ref}}{R_f} \quad (D.5)$$

The value of V_d , R_{load} , R_f are fixed, but V_{ref} can vary. Therefore to calculate the maximum power that the MOSFET has to dissipate we take the derivative of [Equation D.5](#), then we obtain [Equation D.6](#). When setting $\frac{dP}{dV_{ref}} = 0$ and rewriting the equation we obtain [Equation D.9](#). To determine if the maximum or minimum power is calculated, we take the second derivative of the power to V_{ref} which can be found in [Equation D.10](#). The result from this equation is always negative for positive values of R_{load} and R_f , which means that the maximum power is calculated.

$$\frac{dP}{dV_{ref}} = \frac{1}{R_f} \left(V_d - \frac{V_{ref}}{R_f} R_{load} - V_{ref} \right) - \frac{V_{ref}}{R_f} \left(\frac{R_{load}}{R_f} + 1 \right) \quad (D.6)$$

$$0 = \frac{1}{R_f} \left(V_d - \frac{V_{ref}}{R_f} R_{load} - V_{ref} \right) - \frac{V_{ref}}{R_f} \left(\frac{R_{load}}{R_f} + 1 \right) \quad (D.7)$$

$$\left(\frac{2R_{load}}{R_f} + 2 \right) V_{ref} = V_d \quad (D.8)$$

$$V_{ref} = \frac{1}{2} \frac{V_d R_f}{R_{load} + R_f} \quad (D.9)$$

$$\frac{dP^2}{d^2V_{ref}} = \frac{1}{R_f} \left(-\frac{R_{load}}{R_f} - 1 \right) + \frac{1}{R_f} \left(-\frac{R_{load}}{R_f} - 1 \right) \quad (D.10)$$

$$= -\frac{1}{R_f} \left(\frac{R_{load}}{R_f} + 1 \right) \quad (D.11)$$

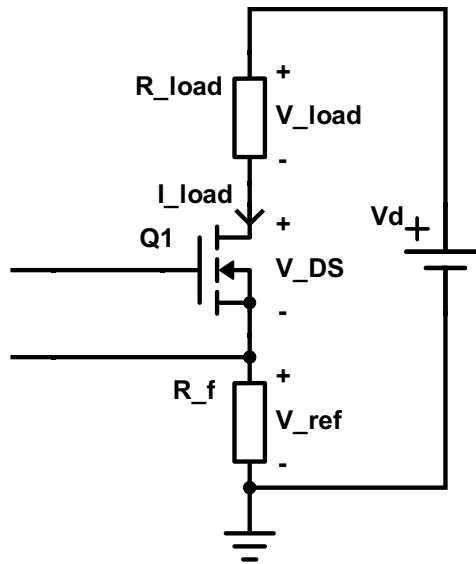
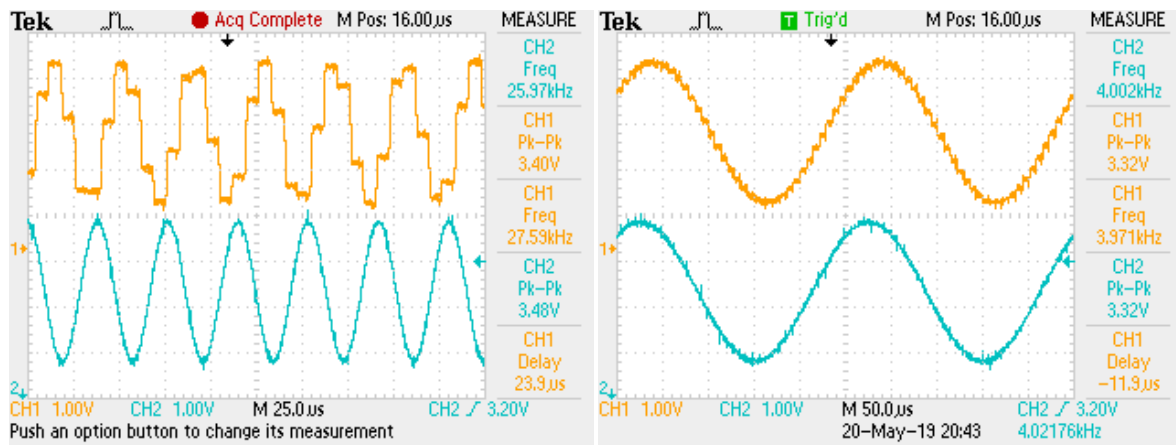


Figure D.1: Circuit for the calculation of power dissipation of the MOSFET

E

DAC measurements

The DAC is tested by having a sinusoid at the input of an ADC which sends the signal to DAC which can be found in [Figure E.1a](#) and [Figure E.1b](#). The signal to ADC is shown as a blue line and the output of the DAC is shown as the yellow line. The frequency in [Figure E.1a](#) is 30 kHz and in [Figure E.1b](#) is 4 kHz.



(a) DAC measurement with 30 kHz

(b) DAC measurement with 4 kHz

Figure E.1: DAC measurements

F

Equipment

Table F.1: Overview of the equipment used for the evaluation of the circuit

Brand	Model
Tektronix	TDS 2022C Two channel digital storage oscilloscope
Tektronix	AFG3021C Single Channel Arbitrary/Function generator
Tektronix	PWS4205 Programmable DC Power Supply 0-20V, 5A
Fluke	177 True RMS Multimeter
Keithley	2450 SourceMeter
digimess	RLC 200 Programmable Automatic RLC Meter

Bibliography

- [1] J. Bouwmeester and J. Guo, “Survey of worldwide pico- and nanosatellite missions, distributions and subsystem technology”, *Acta Astronautica*, vol. 67, no. 7, pp. 854–862, 2010, ISSN: 0094-5765. DOI: <https://doi.org/10.1016/j.actaastro.2010.06.004>. [Online]. Available: <http://www.sciencedirect.com/science/article/pii/S0094576510001955>.
- [2] E. Kulu, *Nanosats database*. [Online]. Available: www.nanosats.eu.
- [3] “Nasa technology roadmaps”, *TA 2: In-Space Propulsion Technologies*, 2015.
- [4] K. Lemmer, “Propulsion for cubesats”, *Acta Astronautica*, vol. 134, pp. 231–243, 2017, ISSN: 0094-5765. DOI: <https://doi.org/10.1016/j.actaastro.2017.01.048>. [Online]. Available: <http://www.sciencedirect.com/science/article/pii/S0094576516308840>.
- [5] M. A. Silva, D. C. Guerrieri, A. Cervone, and E. Gill, “A review of mems micropropulsion technologies for cubesats and pocketqubes”, *Acta Astronautica*, vol. 143, pp. 234–243, 2018, ISSN: 0094-5765. DOI: <https://doi.org/10.1016/j.actaastro.2017.11.049>. [Online]. Available: <http://www.sciencedirect.com/science/article/pii/S0094576517304290>.
- [6] M. A. Silva, D. C. Guerrieri, H. van Zeijl, A. Cervone, and E. Gill, “Vaporizing liquid microthrusters with integrated heaters and temperature measurement”, *Sensors and Actuators A: Physical*, vol. 265, pp. 261–274, 2017, ISSN: 0924-4247. DOI: <https://doi.org/10.1016/j.sna.2017.07.032>. [Online]. Available: <http://www.sciencedirect.com/science/article/pii/S0924424717306490>.
- [7] D. Selva and D. Krejci, “A survey and assessment of the capabilities of cubesats for earth observation”, *Acta Astronautica*, vol. 74, pp. 50–68, 2012, ISSN: 0094-5765. DOI: <https://doi.org/10.1016/j.actaastro.2011.12.014>. [Online]. Available: <http://www.sciencedirect.com/science/article/pii/S0094576511003742>.
- [8] A. Cervone, B. Zandbergen, J. Bouwmester, and J. Guo, “Micro-propulsion research; challenges towards future nano-satellite projects”, *Leonardo Times*, 2013. [Online]. Available: <http://resolver.tudelft.nl/uuid:c1757611-8f73-4061-a573-d748aaa36b23>.
- [9] A. Tummala and A. Dutta, “An overview of cube-satellite propulsion technologies and trends”, *Aerospace*, vol. 4, Dec. 2017. DOI: [10.3390/aerospace4040058](https://doi.org/10.3390/aerospace4040058).
- [10] A. Cervone, B. Zandbergen, D. C. Guerrieri, M. De Athayde Costa e Silva, I. Krusharev, and H. van Zeijl, “Green micro-resistojet research at delft university of technology: New options for cubesat propulsion”, *CEAS Space Journal*, vol. 9, no. 1, pp. 111–125, Mar. 2017, ISSN: 1868-2510. DOI: [10.1007/s12567-016-0135-3](https://doi.org/10.1007/s12567-016-0135-3). [Online]. Available: <https://doi.org/10.1007/s12567-016-0135-3>.
- [11] J. Tsai and L. Lin, “Transient thermal bubble formation on polysilicon micro-resistors”, *Journal of Heat Transfer*, vol. 124, pp. 375–382, 2002. DOI: [10.1115/1.1445136](https://doi.org/10.1115/1.1445136).
- [12] K. T. Wen-Jei Yang, “Overview of boiling on microstructures - macro bubbles from micro heaters”, *Microscale Thermophysical Engineering*, vol. 4, no. 1, pp. 7–24, 2000. DOI: [10.1080/108939500199600](https://doi.org/10.1080/108939500199600). eprint: <https://doi.org/10.1080/108939500199600>. [Online]. Available: <https://doi.org/10.1080/108939500199600>.
- [13] R. M. Stitt, *Implementation and application of current sources and current receivers*, Texas Instruments, 1990.
- [14] R. M. Stitt, *Make a precision current source or current sink*, Texas Instruments, 1994.
- [15] L. T. Harrison, *Current Sources and Voltage References*. Elsevier, 2005.
- [16] T. Van Wees, “Characterization and testing of a mems-vaporizing liquid microthruster for small satellite propulsion”, Master’s thesis, Delft University of Technology, 2017.
- [17] R. M. Fox, S.-G. Lee, and D. T. Zweidinger, “The effects of bjt self-heating on circuit behavior”, *IEEE Journal of Solid-State Circuits*, vol. 28, no. 6, pp. 678–685, Jun. 1993, ISSN: 0018-9200. DOI: [10.1109/4.217983](https://doi.org/10.1109/4.217983).

- [18] Y. Wang, N. Li, H. Yu, Z. Sun, H. Nie, and H. Xu, "Study on wide-band voltage controlled current source for electrical impedance tomography", in *2012 Second International Conference on Intelligent System Design and Engineering Application*, Jan. 2012, pp. 1499–1502. DOI: [10.1109/ISdea.2012.616](https://doi.org/10.1109/ISdea.2012.616).
- [19] *A comprehensive study of the howland current pump*, Texas Instrument, 2008.
- [20] H. Hong, M. Rahal, A. Demosthenous, and R. H. Bayford, "Comparison of a new integrated current source with the modified howland circuit for EIT applications", *Physiological Measurement*, vol. 30, no. 10, pp. 999–1007, Aug. 2009. DOI: [10.1088/0967-3334/30/10/001](https://doi.org/10.1088/0967-3334/30/10/001). [Online]. Available: <https://doi.org/10.1088/0967-3334/30/10/001>.
- [21] B. Ferreira and W. Van der Merwe, *The Principles of Electronic and Electromechanic Power Conversion: A Systems Approach*. Wiley/IEEE, 2014, ISBN: 9781118798843.
- [22] M. Gaboriault and A. Notman, "A high efficiency, noninverting, buck-boost dc-dc converter", in *Nineteenth Annual IEEE Applied Power Electronics Conference and Exposition, 2004. APEC '04.*, vol. 3, Feb. 2004, 1411–1415 Vol.3. DOI: [10.1109/APEC.2004.1296049](https://doi.org/10.1109/APEC.2004.1296049).
- [23] C. Straathof and R. van Wijk, "Measuring device for controlling a vaporising microthruster", (to appear), 2019.
- [24] M. Rebers and G. Breysens, "Control and data-acquisition of a heater/temperature sensor", (to appear), 2019.
- [25] A. J. Montagne, *Structured Electronic Design*, 1.1. Delft Academic Press, 2018, ISBN: 9065624279.